LEVEL II

(12)
B.S.

MISCELLANEOUS PAPER GL-80-5

INTERPRETATION OF DATA FROM UPHOLE REFRACTION SURVEYS

AD A087775

by

Arley G. Franklin

Geotechnical Laboratory
U. S. Army Engineer Waterways Experiment Station
P. O. Box 631, Vicksburg, Miss. 39180

June 1980
Final Report

Approved For Public Release; Distribution Unlimited

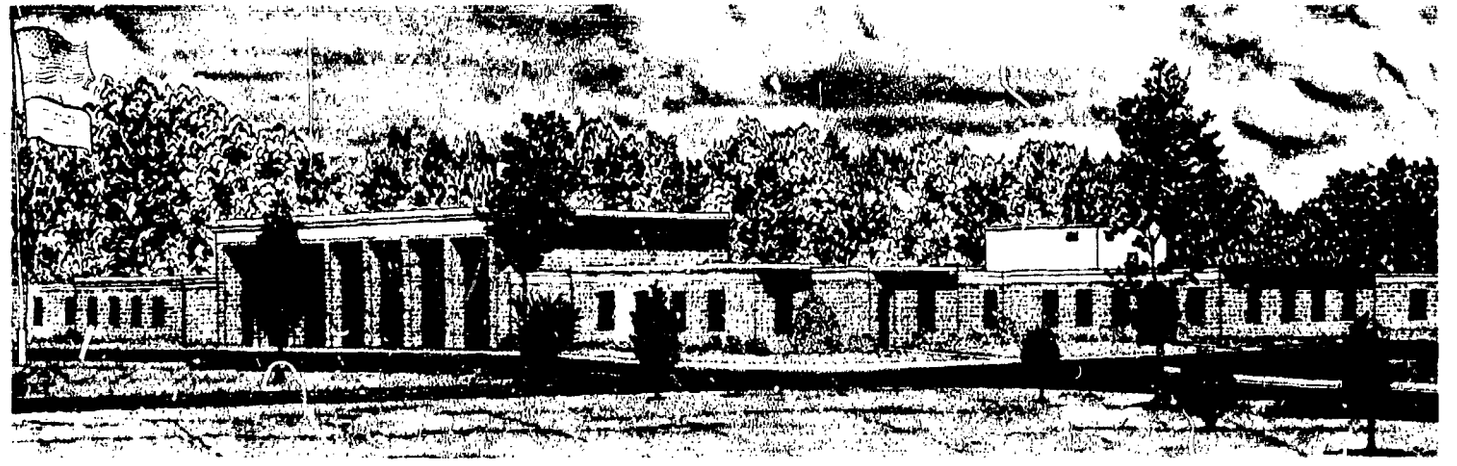

Prepared for Office, Chief of Engineers, U. S. Army
Washington, D. C. 20314

Under CWIS Work Unit 31150

DDC FILE COPY

DTIC
ELECTE
AUG 1 2 1980
S D
A

80 8 11 076

Destroy this report when no longer needed. Do not return it to the originator.

The findings in this report are not to be construed as an official Department of the Army position unless so designated by other authorized documents.

Unclassified

SECURITY CLASSIFICATION OF THIS PAGE (When Data Entered)

REPORT DOCUMENTATION PAGE

READ INSTRUCTIONS BEFORE COMPLETING FORM

1. REPORT NUMBER: Miscellaneous Paper GL-
2. GOVT ACCESSION NO.: AD-A087 775
3. RECIPIENT'S CATALOG NUMBER:
4. TITLE (and Subtitle): INTERPRETATION OF DATA FROM UPHOLE REFRACTION SURVEYS
5. TYPE OF REPORT & PERIOD COVERED: Final report
6. PERFORMING ORG. REPORT NUMBER:
7. AUTHOR(s): Arley G. Franklin
8. CONTRACT OR GRANT NUMBER(s): Jun 80
9. PERFORMING ORGANIZATION NAME AND ADDRESS: U. S. Army Engineer Waterways Experiment Station, Geotechnical Laboratory, P. O. Box 631, Vicksburg, Miss. 39180
10. PROGRAM ELEMENT, PROJECT, TASK AREA & WORK UNIT NUMBERS: CWIS Work Unit 31150
11. CONTROLLING OFFICE NAME AND ADDRESS: Office, Chief of Engineers, U. S. Army, Washington, D. C. 20314
12. REPORT DATE: June 1980
13. NUMBER OF PAGES: 68
14. MONITORING AGENCY NAME & ADDRESS (if different from Controlling Office): WES/MP/GL-80-5
15. SECURITY CLASS. (of this report): Unclassified
15a. DECLASSIFICATION/DOWNGRADING SCHEDULE:

16. DISTRIBUTION STATEMENT (of this Report)

Approved for public release; distribution unlimited.

17. DISTRIBUTION STATEMENT (of the abstract entered in Block 20, if different from Report)

18. SUPPLEMENTARY NOTES

19. KEY WORDS (Continue on reverse side if necessary and identify by block number)

Refraction
Uphole refraction
Seismic refraction
Seismic refraction method
Seismic surveys
Subsurface exploration

20. ABSTRACT (Continue on reverse side if necessary and identify by block number)

The conventional interpretation of the data from an uphole refraction survey is based on the similarity between a plot of contours drawn on uphole arrival times and a wave-front diagram, which shows successive positions of the wave front produced by a single shot location at the ground surface. However, the two are alike only when the ground consists solely of homogeneous strata, oriented either horizontally or vertically. In this report, the term "Meissner diagram" is used for the plot of arrival times from the uphole -

(Continued)

DD FORM 1 JAN 73 1473 EDITION OF 1 NOV 65 IS OBSOLETE

Unclassified

SECURITY CLASSIFICATION OF THIS PAGE (When Data Entered)

4/11/23, vdk

20. ABSTRACT (Continued)

refraction survey in order to maintain the distinction between it and a true wave-front diagram.

Where departures from the case of homogeneous, horizontal strata exist, the interpretation of the Meissner diagram is not straightforward, although a partial interpretation in terms of a horizontally stratified system is usually possible. A systematic approach to the interpretation problem, making use of such a partial interpretation, is proposed. It consists of: (a) determination of a tentative set of layer velocities and thicknesses on the basis of the wave-front interpretation; (b) computation of theoretical travel times for the uphole refraction survey with these layer parameters; (c) generation of an anomaly diagram by contouring the differences between observed and theoretical travel times; and (d) identification of causative geological features by comparison with anomaly diagrams representing known or hypothesized geological conditions.

Meissner diagrams and companion anomaly diagrams are presented for cases of subsurface cavities of different sizes in rock of different velocities, ridges and depressions on the bedrock surface, vertical offsets, dipping strata, and various errors of interpretation and measurement. Examples of field data from two sites are presented. Algorithms for computer generation of Meissner diagrams and anomaly diagrams are presented in Appendix A.

On the basis of the studies described, it is concluded that the interpretation of uphole refraction data can be aided by the use of anomaly diagrams and that the nature of many geological features may be identified by comparison with anomaly diagrams representing hypothetical cases. While seismic travel times are affected by the presence of subsurface cavities and large cavities are identifiable, the sensitivity of the method is marginal for practical use in cavity detection. Some cavities large enough to be of engineering significance (e.g., a tunnel of 4-m diameter) may be practically undetectable by this method.

PREFACE

The study reported herein was performed by the U. S. Army Engineer Waterways Experiment Station (WES) as a part of the Civil Works research effort of the Office, Chief of Engineers (OCE), U. S. Army. The work was conducted as a task under the CWIS Work Unit 31150, "Remote Delineation of Cavities and Discontinuities in Rock," which is monitored for OCE by Mr. Paul Fisher.

The study was conducted and the report prepared by Dr. Arley G. Franklin of the Earthquake Engineering and Geophysics Division (EE&GD), Geotechnical Laboratory (GL). General supervision was provided by Dr. Paul F. Hadala, Chief, EE&GD, and Mr. James P. Sale, Chief, GL.

COL John L. Cannon, CE, and COL Nelson P. Conover, CE, were Commanders and Directors of WES. Mr. Fred R. Brown was Technical Director.

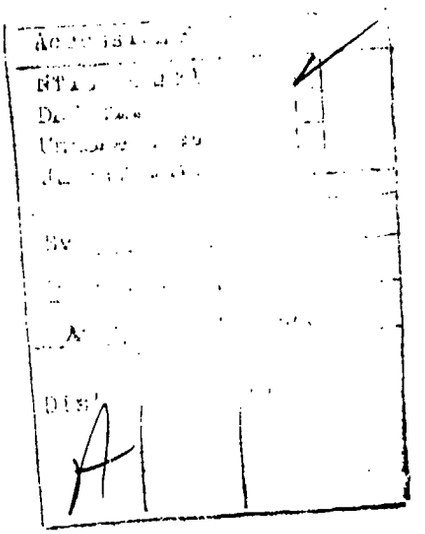

CONTENTS

	Page
PREFACE	1
CONVERSION FACTORS, U. S. CUSTOMARY TO METRIC (SI) UNITS OF MEASUREMENT	3
PART I: INTRODUCTION	4
Background	4
Purposes of Study	5
PART II: TRAVEL TIME DIAGRAMS	6
Wave-Front Diagrams	6
Meissner Diagrams	11
PART III: INTERPRETATION OF THE MEISSNER DIAGRAM	15
Discussion	15
Examples	19
Cavities	19
Irregularities of the layer boundaries	21
Offset in bedrock surface	26
Dipping strata	30
Errors in measurement and interpretation	34
Measurement errors	34
Resolution of layer boundaries	34
Errors in interpretation of velocity	36
Errors in location of layer boundaries	37
PART IV: EXAMPLES OF FIELD DATA	39
Arizona Site	39
Waterways Experiment Station Site	43
PART V: SUMMARY AND CONCLUSIONS	46
Summary	46
Conclusions	47
REFERENCES	49
APPENDIX A: COMPUTER-AIDED GENERATION OF WAVE-FRONT AND MEISSNER DIAGRAMS	A1

CONVERSION FACTORS, U. S. CUSTOMARY TO METRIC (SI) UNITS OF MEASUREMENT

U. S. customary units of measurement used in this report can be converted to metric (SI) units as follows:

Multiply	By	To Obtain
degrees (angle)	0.01745329	radians
feet	0.3048	metres
feet per second	0.3048	metres per second
pounds (mass)	0.45459237	kilograms

INTERPRETATION OF DATA FROM UPHOLE REFRACTION SURVEYS

PART I: INTRODUCTION

Background

1. The uphole refraction method of subsurface exploration uses a seismic signal generated at some depth in a borehole (usually by an explosive charge) and detected at the various geophones of a surface array that extends in a straight line away from the borehole. The method provides the same information as the surface refraction method and adds to it observations of the effects of vertical displacements of the shot point. Thus, it provides another dimension in the information obtained about ground conditions. The method offers a prospect for the detection of subsurface cavities, since cavities can be expected to influence the transit times of seismic signals whose ray paths they intercept. It also provides a way of identifying and defining velocity reversals--cases in which a stratum has a lower velocity than that of the overlying material and which cannot be identified by surface refraction surveys--as well as other subsurface conditions that would be obscure to an observer confined to the surface.

2. Conventional interpretation of the plot of the seismic travel times from an uphole refraction survey is based on the similarity of the plot to a wave-front diagram for a single shot at the ground surface. This similarity was pointed out by Meissner (1961), and such efforts are sometimes called "Meissner wave-front surveys." The similarity, however, is true only if the ground consists of homogeneous strata, oriented either horizontally or vertically. Correct interpretation is not straightforward when inhomogeneities or departures from this ideal geometry occur.

Purposes of Study

3. The primary purposes of the present investigation are to gain some insight for the interpretation of uphole refraction data through the study of hypothetical data that would be obtained under various simple, but nonideal, geological conditions, and to propose a systematic approach to the interpretation problem. An additional purpose is to evaluate, in an approximate manner, the sensitivity of the method to the presence of subsurface cavities and the potential of the method for use in cavity detection.

PART II: TRAVEL TIME DIAGRAMS

Wave-Front Diagrams

4. To develop the concept of the wave-front diagram and its physical meaning, consider the propagation of a seismic wave through the ground after the detonation of an explosive charge at the ground surface (Figure 1). The disturbance propagates outward from the source with a velocity that is determined by the elastic properties of the medium. If the source is considered to be a single point and the medium surrounding it to have a constant seismic velocity v, then at some time t after the event occurs the disturbance will have traveled a distance s, where

$$s = vt \tag{1}$$

More generally,

$$ds = v\,dt \tag{2}$$

where ds and dt are differential increments of distance and time. The boundary between the region in which the disturbance has been felt and the region that is still undisturbed is the wave front corresponding to time t.

5. The wave-front diagram in Figure 1 depicts the successive position of the wave front at intervals of 2 msec. The surficial layer shown has a seismic velocity of 2000 ft/sec (610 m/sec) and a thickness of 10 ft (3 m). The first two wave-front positions, at 2 and 4 msec, are entirely within the first layer and are hemispherical shells 4 ft (1.2 m) apart. Where the disturbance meets a boundary with another medium of different seismic velocity, it is propagated in the second medium with a velocity characteristic of that material's elastic properties. In Figure 1, the velocity v_2 of the second layer is 6000 ft/sec (1830 m/sec) and the distance between successive wave-front positions at 2-msec intervals is therefore 12 ft (3.7 m).

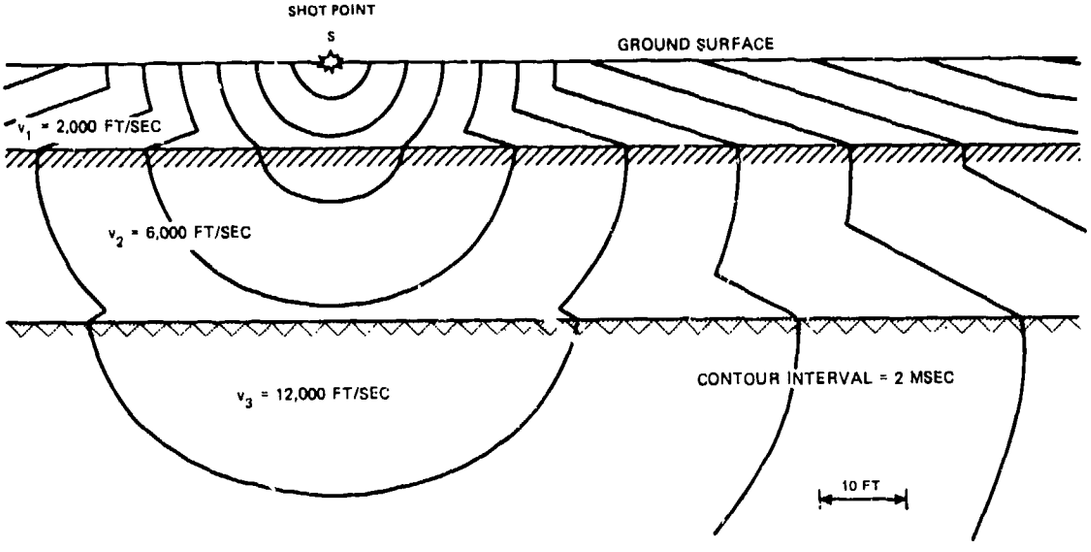

Figure 1. Wave-front diagram, showing wave-front positions at 2-msec intervals

6. The wave front in the second layer is not spherical. In general, it has no simple mathematical expression, but is a composite surface. The reason for this is that as far as this layer is concerned, the source of the disturbance is not a point, but a circular area imprinted on the boundary by the wave front advancing from above. The downward-advancing spherical wave front is tangent to the interface at the instant of first contact and shortly afterwards makes a very small angle with the interface in the neighborhood of the point of initial contact. Thus, the radius of the circular imprinted area initially expands with a velocity greater than the seismic velocity of either medium. In Figure 2, this velocity is shown as v_c. It is given by

$$v_c = \frac{v_1}{\sin \theta} \tag{3}$$

where v_1 is the velocity of the advancing wave front and θ is the angle between the wave front and the interface of the contact. As the area of contact increases, the contact angle θ also increases, so

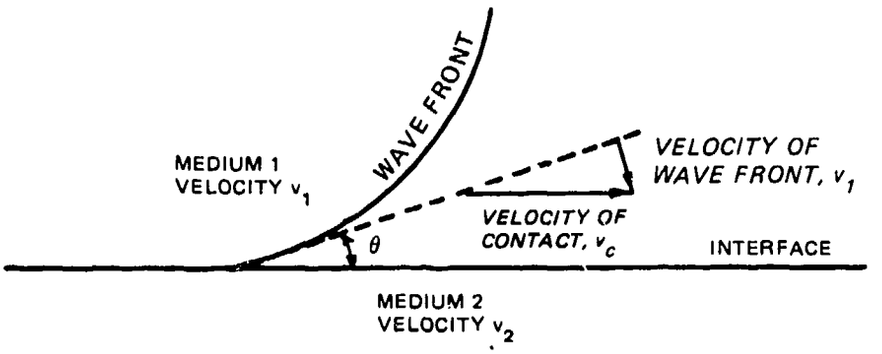

Figure 2. Velocity of wave front-interface contact

that the velocity v_c diminishes. When v_c finally equals v_2, the velocity of the second layer, then

$$\sin \theta_c = \frac{v_1}{v_2} \tag{4}$$

which can be recognized as the expression of Snell's law for the case of critical incidence. The subscript c is added to θ to indicate that it represents the critical angle of incidence. This occurs at a horizontal distance d from the shot point, such that

$$d = H_1 \tan \theta_c \tag{5}$$

where H_1 is the thickness of the first layer.

7. At distances greater than d, the disturbance moves through the upper part of layer 2 with a velocity v_2, generating a disturbance in layer 1 that outruns the spherical wave front advancing with velocity v_1. This wave, known as a "head wave," is conical in shape and its successive positions are therefore represented by straight lines in the cross section of Figure 1. The perpendicular distance between the successive positions of the head wave is, according to Equation 2,

equal to $v_1\Delta t$, where Δt is the time interval. The distance along the interface, however, is $v_2\Delta t$, and the head wave therefore makes the angle θ_c with the interface.

8. Similar phenomena can be seen at the interface between layer 2 and layer 3, including a head wave in layer 2. At the extreme right side of the figure, a second head wave can be seen in layer 1, as a result of the arrival of the head wave from layer 3 at the interface between layers 1 and 2. By following the head wave from layer 3 up through layer 2 and into layer 1, one can see that the distance between successive wave-front positions along the interface is equal to $v_3\Delta t$. The distance perpendicular to the wave front is $v_1\Delta t$; so the angle between the wave front and the interface is equal to $\sin^{-1}(v_1/v_3)$.

9. A wave-front diagram can be constructed for any combination and any configuration of subsurface materials by straightforward application of Equation 2 and Huygens' principle, which states that each point of an advancing wave front constitutes a new center of disturbance from which new wavelets emanate, and the envelope of these wavelets at a later instant in time is a new wave front. Huygens' principle is the basis of Snell's law, which describes the phenomenon of refraction at an interface. It also is the guiding principle for construction of the wave-front diagram around a nontransmitting body such as an empty cavity; i.e., for diffraction of the wave. The construction of wave-front diagrams and their use in interpretation of seismic refraction data is further described by Thornburgh (1930) and Rockwell (1967).

10. The wave-front diagram shows the successive positions of the wave front at different instants in time, and conversely it shows for any point in the cross section the time required for the first disturbance to reach that point. A wave-front diagram can therefore be constructed from field data by drawing contours of equal arrival time, using interpolation between times measured at a sufficient number of seismic detectors buried at various depths and distances from the source. Examples of such experiments are given by Murrell (1973, 1974). For computer generation of hypothetical wave-front diagrams, the seismic

travel times can be computed for a number of discrete grid points in the cross section, and contoured in the same way. A computer-generated wave-front diagram, for the same cross section as in Figure 1, is shown in Figure 3. The points at which arrival times were computed are shown by dots on the diagram; they are on a 5-ft (1.5-m) spacing. This spacing is the primary factor in controlling the degree to which fine detail can be resolved. The computer algorithms used to compute the times and to plot the contours are described in Appendix A.

11. The interpretation of the wave-front diagram for the case of horizontally stratified soils or rocks follows the same principles as the construction of a wave-front diagram. The layer velocities are given by the spacing between successive contours, measured along the normal to the contours. If the contour interval is Δt and the spacing between contours is Δs, then the seismic wave velocity v of the layer is

$$v = \frac{\Delta s}{\Delta t} \tag{6}$$

The layer boundaries are determined as the horizontal lines on which the velocity changes occur or where the directions of contours change abruptly. (Abrupt direction changes also occur at the intersections of direct waves and head waves, but these are not aligned horizontally.)

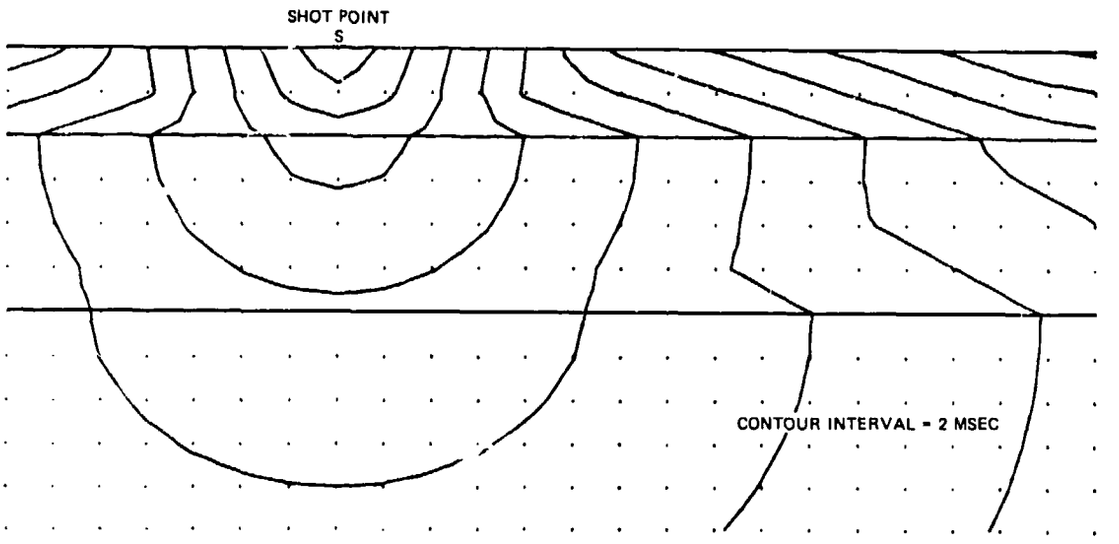

Figure 3. Wave-front diagram generated by drawing contours on computed travel time values at grid points; same cross section as shown in Figure 1

Meissner Diagrams

12. Under some conditions a wave-front diagram can be simulated by a plot of data obtained from uphole refraction shooting (Meissner 1961). An uphole refraction survey is carried out as shown schematically in Figure 4. A shot is fired at some depth in a borehole, and the time required for the disturbance to reach each of a number of geophones on the ground surface is measured. The process is repeated for shot points at various depths. Consider the travel time for a particular combination of shot point S and receiver R , and for a fictitious buried receiver R' , located at the same depth as S and directly beneath R . If the subsurface materials consist only of horizontal, homogeneous strata, it is obvious from the symmetry of the actual and

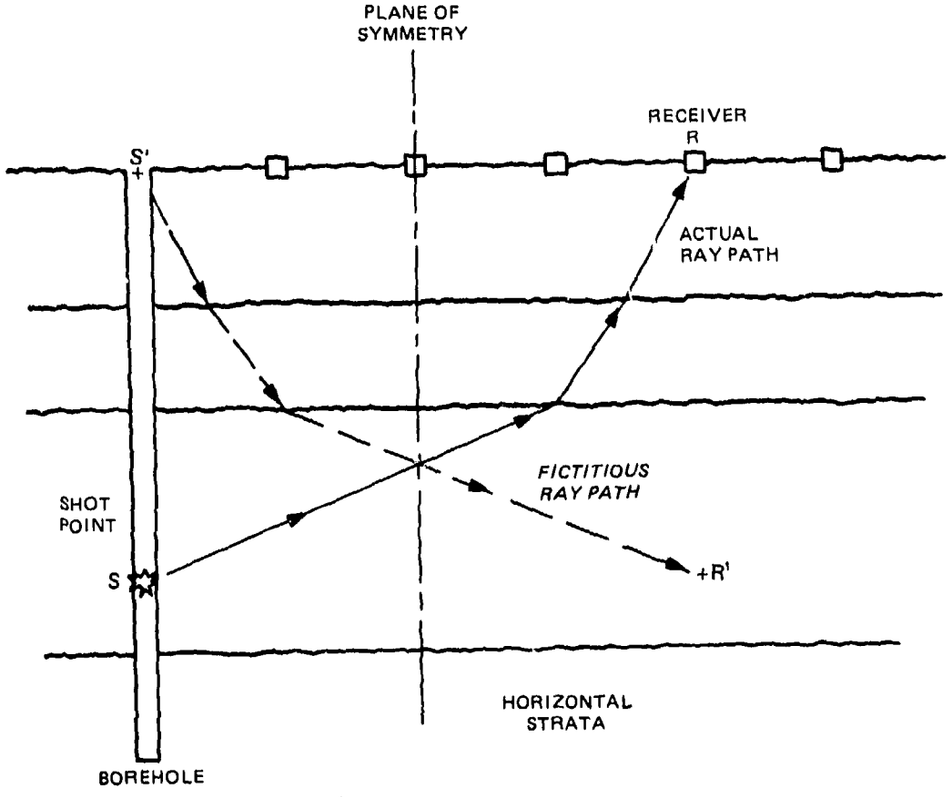

Figure 4. Uphole refraction survey

fictitious ray paths in Figure 4 that the seismic travel times for those two paths must be equal. (The symmetry, and thus the time equality, will also hold in the infrequent case of a subsurface configuration consisting only of vertically oriented strata.) On a cross section, a grid point is plotted for each shot point-receiver combination, at the shot point depth and the receiver distance. The seismic travel time for each combination is assigned to its grid point, and a contour plot, or map, of the time values is drawn by conventional map contouring methods.

13. A plot of contours on uphole refraction times will be called a "Meissner diagram" in this report. It is important to make a clear distinction between a Meissner diagram and a wave-front diagram because the two are the same only in the special case of uniform horizontal (or vertical) strata. This point is illustrated by Figure 5, which shows for comparison a wave-front diagram (Figure 5a) and a Meissner diagram (Figure 5b) for a hypothetical situation in which the survey is made across a long cavity, 10 ft (3 m) high by 60 ft (18 m) wide. Both diagrams are made with the assumption that the cavity is empty (i.e., air-filled) and that no detectable seismic wave is transmitted through it. It is clear from this comparison that the Meissner diagram is not a true wave-front diagram in this instance. This is generally true wherever the symmetry condition illustrated in Figure 4 does not hold.

14. In particular, anomalies in the Meissner diagram should not be interpreted on the basis of the wave-front analogy, since it is precisely in those areas that the analogy most seriously breaks down. Moreover, it is also apparent from Figure 5b that the area of the anomaly in the Meissner diagram does not coincide with the location of the feature responsible for it. That this should be expected is evident from consideration of Figure 4 and the significance of the time value plotted at point R' . This is the time required for the seismic signal to travel from S to R , which depends only on the conditions along the ray path between those points. It conveys no direct information about conditions at point R' , where it is plotted. In general, the Meissner diagram reveals nothing about the materials or conditions

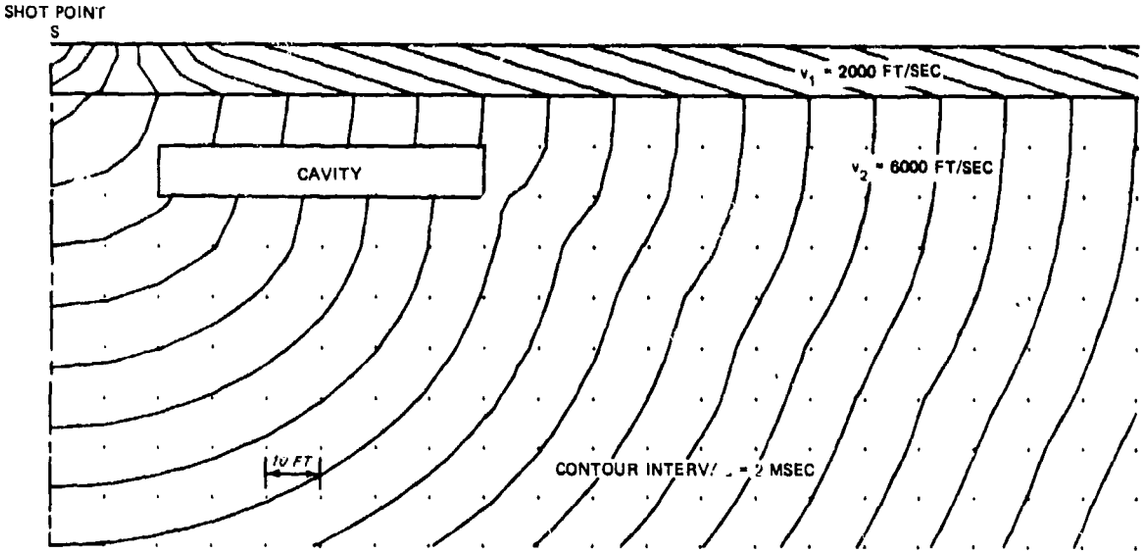

a. WAVE-FRONT DIAGRAM

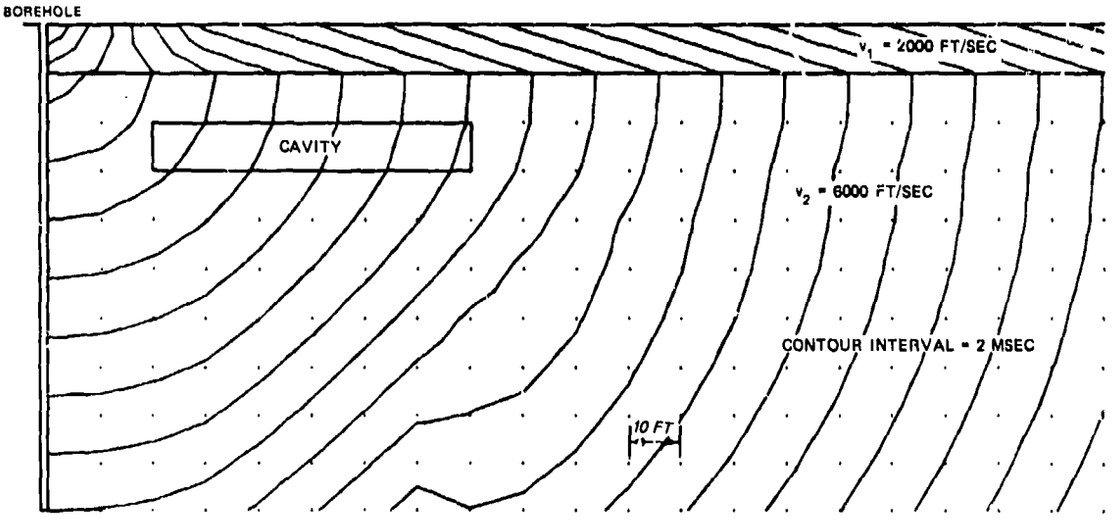

b. MEISSNER DIAGRAM

Figure 5. Comparison of wave-front diagram and Meissner diagram for a cross section containing a 10-ft by 60-ft cavity

below the ray path from the deepest shot point to the most distant geophone, or, roughly, the diagonal across the diagram.

15. It is more satisfying to view the Meissner diagram as a means of displaying and interpreting data obtained in an uphole refraction

survey than as an imperfect simulation of a wave-front diagram. The uphole refraction method produces more information about subsurface conditions than does the surface refraction method and thus offers the possibility of detecting features that are invisible to surface refraction methods. The data from the uphole refraction survey, however, need to be displayed in a two-dimensional frame of reference, and the Meissner diagram provides a way to do this. Furthermore, as Figure 5 illustrates, while interpretation of anomalies in the Meissner diagram is not straightforward, an initial partial interpretation of the data can be made on the basis of the wave-front analogy, if anomalies are provisionally ignored. Thus, a wave-front interpretation of Figure 5b would be adequate to define the layer boundary and the layer velocities, at least to an acceptable degree of approximation. This may be followed by a more detailed interpretation in which the nature of the anomalies is considered.

PART III: INTERPRETATION OF THE MEISSNER DIAGRAM

Discussion

16. If the gross features of the Meissner diagram conform to those of a wave-front diagram for a horizontally layered system, a first step in interpretation consists of picking layer boundaries and measuring average layer velocities on the basis of the wave-front diagram. It then remains to interpret the significance of anomalies that appear in the Meissner diagram. The term "anomaly" means, in this context, a travel time or a pattern of travel times that is not compatible with the geological model currently being used for interpretation or for comparison. At this stage of interpretation, then, anomalies are features in the contour pattern that are not compatible with a wave-front diagram for a horizontally layered system.

17. The layer velocity is calculated from the spacing between contours, measured along the normal, as shown in Equation 6. An average layer velocity can be determined from an average contour spacing over a broad area of the diagram, or a more precise value of layer velocity may be available from contour spacing in areas of the diagram that are not affected by anomalous features.

18. An analytical basis for the interpretation of anomalies in the Meissner diagram is lacking. However, one available approach is to hypothesize a set of subsurface conditions (e.g., those shown in Figure 5b) thought to be appropriate to the problem, to construct a synthetic Meissner diagram, and to compare that diagram with the Meissner diagram obtained from field data. Such an interpretation will be essentially qualitative. The comparison of the hypothetical and the experimental Meissner diagrams will indicate whether the nature of the geological anomaly has been correctly identified and will give some indication of its magnitude. It is not to be expected that an accurate description of the size and shape of the anomalous feature will be obtained, but it can be described in terms of its effect on the seismic

travel times. Obviously, where multiple anomalies are present and they interact in their effect on seismic travel times, interpretation will be both more difficult and more uncertain.

19. Construction of a synthetic Meissner diagram is straightforward, if tedious. Since the diagram is to be constructed by drawing contours on the seismic travel time values, the problem reduces to computing the travel time for any chosen source-detector combination. The travel time considered is that of the first-arriving signal; so the procedure is simply to find among all of the possible propagation paths through the various transmitting media, and around any nontransmitting barriers, the one path that yields the smallest travel time. An example is shown in Figure 6. The cavity is assumed to be empty and nontransmitting. (The assumption is justified by the low compression wave velocity of air, which is about 1100 ft/sec (330 m/sec), and the probable low degree of acoustic coupling between the air and the surrounding rock.) Three ray paths that are considered are shown. Path A is the one that would govern if the cavity were not present. It is evident

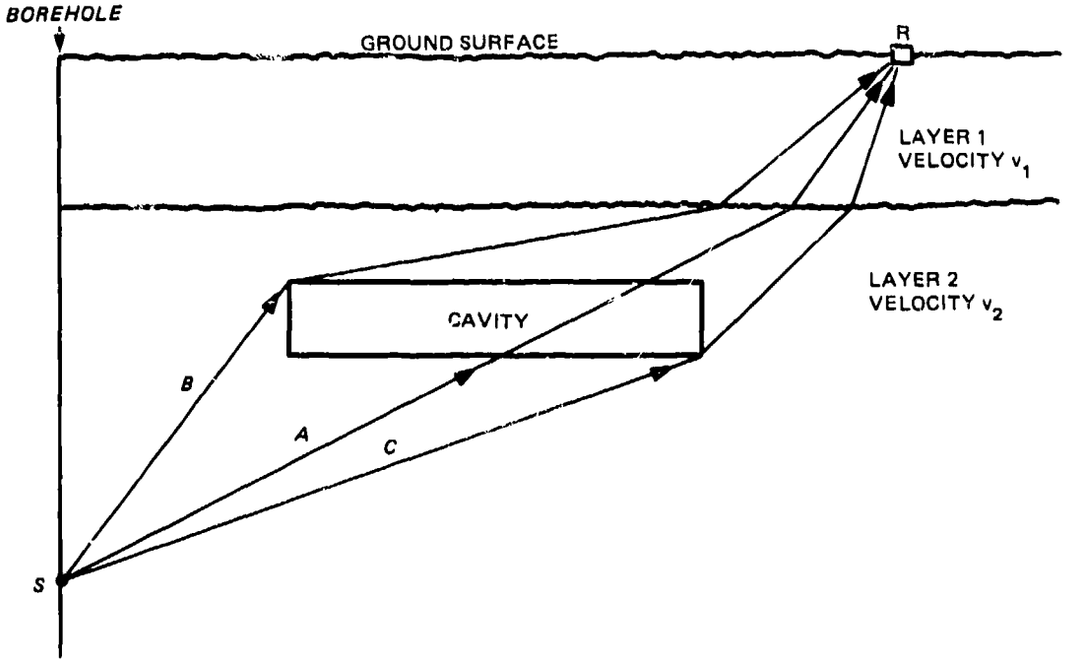

Figure 6. Computation of travel time around an empty cavity

that a cavity located so that it did not intercept Path A would not affect the first-arrival time, though with the cavity as shown, Path A is not a possible ray path. Paths B and C appear to be roughly equivalent, so that the travel times should be computed for both paths and the shorter time chosen. It is apparent by inspection that any more circuitous path would require a greater time for the signal to reach R . For other geological conditions, similar reasoning is applied. In all cases, the path of minimum travel time is such that: (a) Snell's law is satisfied wherever the path crosses a boundary between media with different velocities; (b) the path within any one homogeneous, isotropic medium is a straight line; and (c) the path around a nontransmitting barrier is one of minimum distance. Snell's law states that

$$\frac{\sin i}{\sin r} = \frac{v_1}{v_2} \tag{7}$$

where v_1 and v_2 are the respective seismic propagation velocities of the two media and i and r are the angles of incidence and refraction of the ray path, as shown in Figure 7.

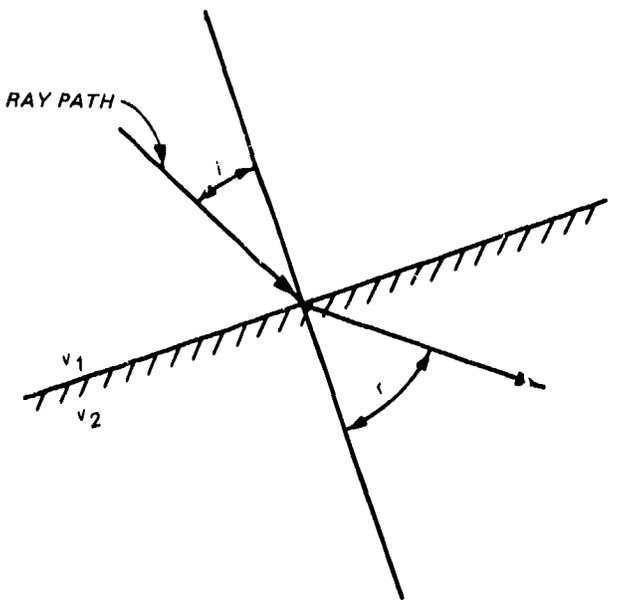

Figure 7. Refraction of ray path at boundary between media with different velocities of wave propagation

20. To gain some insight for interpretation of anomalies in the Meissner diagram and to examine the sensitivity of the uphole refraction method as a means of detecting cavities, travel times have been computed and Meissner diagrams constructed for some simple, two-dimensional, hypothetical cases, including empty cavities beneath the bedrock surface. These examples are presented in subsequent paragraphs. To aid in concentrating more closely on the anomalies themselves, another type of diagram is introduced. This is the anomaly diagram, which is generated by contouring the differences between the travel times of the actual (or hypothetical) Meissner diagram and the travel times that would have occurred with the interpreted set of layers and layer velocities, but without the anomalies. In other words, the anomaly diagram is constructed as follows: (a) the layer boundaries and velocities are determined from the Meissner diagram; (b) the travel times for the ideal layered system consisting of those layers are computed; (c) the computed travel times are subtracted from the measured times; and (d) contours are drawn on the time differences. This requires only a very small additional effort over that involved in conventional interpretation methods, since the computation of travel times for the layered system and the drawing of contours is done by the computer, using the algorithms described in Appendix A.

21. Since the seismic travel times can be computed for any arbitrary distribution of velocities, it is possible in principle to use the computer to generate a Meissner diagram for any hypothesized set of geological conditions, though a computer code to do this is not yet available. Given the availability of such a code, it is possible to visualize an iterative computer-assisted approach to the interpretation problem. First, the field data are displayed in a Meissner diagram. An anomaly diagram is then produced on the basis of the interpreted layer boundaries and velocities. From an examination of the time anomalies, the nature of the geological anomalies is inferred, and a hypothetical Meissner diagram corresponding to the inferred geological conditions is generated. The times for this diagram are

subtracted from the measured times to yield a second generation anomaly diagram. If necessary, the process could be carried on into the third or further generations. The final anomaly diagram, showing that interpretation was complete, would contain no features at all other than a pattern of random measurement errors.

22. It is possibly belaboring the obvious to point out that the geological information obtained in logging the borehole should not be ignored in interpretation of the seismic data. The interpreter should use all available geological information, rather than treating the geophysical interpretation as an isolated academic exercise.

Examples

23. In the succeeding paragraphs, some examples are offered to show the effects of various simple geological features on the Meissner diagram. The travel times for all cases other than simple horizontally stratified systems were computed by hand, using the principles described earlier. For the horizontally stratified system, travel times were obtained with the aid of the computer algorithm described in Appendix A. Both Meissner diagrams and anomaly diagrams were contoured by computer, using the routine described in Appendix A.

24. Points for which travel times were computed are shown by dots in the diagrams. In most cases, the (hypothetical) borehole is at the left side of the diagram, but in any case its position can be identified by the convergence of the travel times to zero at its top. In some instances, contours in the anomaly diagrams have actually been drawn on values very slightly higher or lower than those shown in order to avoid the generation of numerous redundant zero contours in areas of the diagram where the values are all zero. This was not done in diagrams where zero contours are not shown.

Cavities

25. Figure 8a shows a Meissner diagram or wave-front diagram for a system consisting of a bedrock having a compression wave velocity of

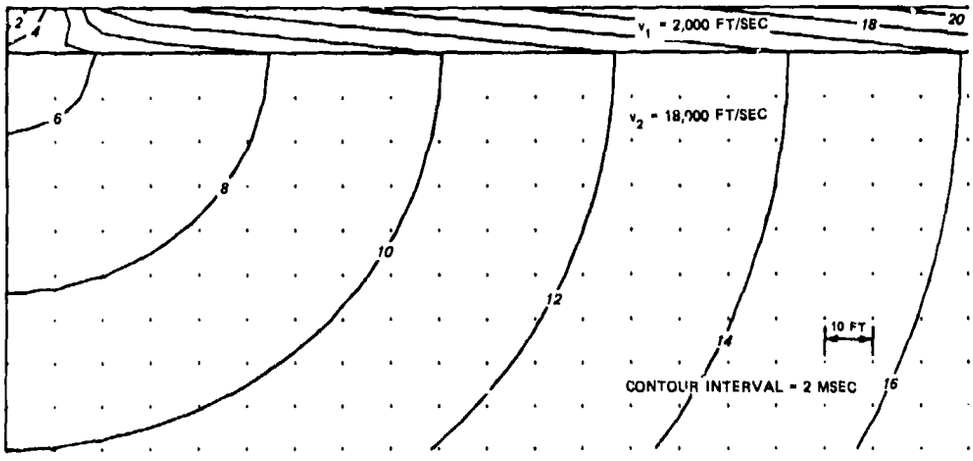

a. MEISSNER DIAGRAM FOR A SIMPLE TWO-LAYER SYSTEM

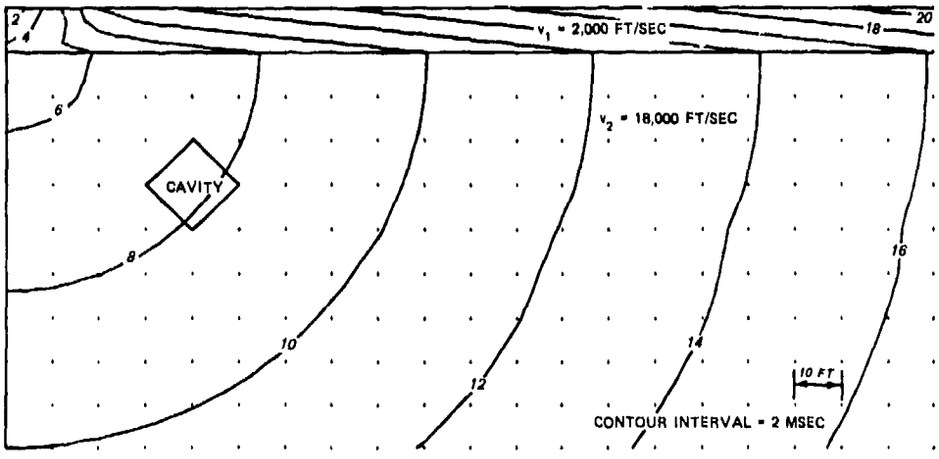

b. MEISSNER DIAGRAM WITH EFFECT OF 14-FT-SQUARE CAVITY

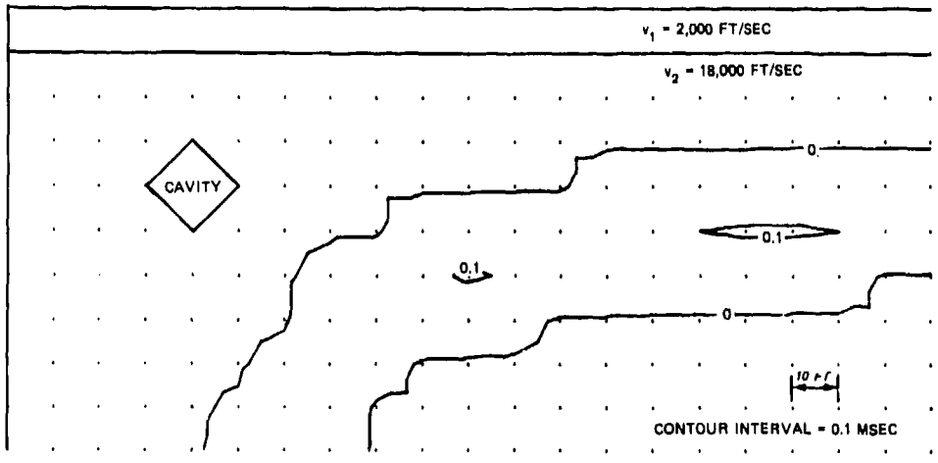

c. ANOMALY DIAGRAM

Figure 8. Effects of a 14-ft-square cavity on Meissner diagram with bedrock of 18,000-ft/sec compression wave velocity

18,000 ft/sec (5,500 m/sec) with a 10-ft- (3-m-) thick overburden layer having a compression wave velocity of 2,000 ft/sec (600 m/sec). A Meissner diagram and anomaly diagram showing the effects of a tunnellike cavity, 14.14-ft- (4.3-m-) square, 20 ft (6 m) below the bedrock surface, are shown in Figures 8b and 8c, respectively. The effect on the Meissner diagram is a scarcely noticeable wiggle in the contours at 12, 14, and 16 msec. The anomaly diagram shows that the total anomaly is a little more than 0.1 msec, which leads one to conclude that a cavity of such size in rock of such velocity is for practical purposes not detectable by means of an uphole refraction survey. However, the character of the anomaly deserves study because larger cavities, or cavities in rocks of lower velocity, may be detectable. The anomaly is seen to be a band, bounded on the left by the position of the nearest geophone whose signal is affected and at the top by the shallowest shot point whose ray paths to the surface are intercepted by the opening. The location of the cavity can be inferred from considerations of this kind, but it is important to note that the locations of the cavity and the resulting time anomaly do not coincide on the diagram.

26. The effect of a larger opening, 10 ft (3 m) high by 60 ft (18 m) wide and in the same 18,000 ft/sec (5,500 m/sec) bedrock, is shown in Figure 9. The anomaly is similar to that in Figure 8, but is larger in both area and time. The total time anomaly in this case is about 0.9 msec, which is on the borderline of practical detectability, considering the normally attainable degree of precision in seismic measurements. In a rock with a velocity three times smaller, the magnitude of the time anomaly is tripled, as shown in Figure 10, but the areal extent and shape of the anomaly is similar.

Irregularities of the layer boundaries

27. A depression in the soil-rock interface has a much stronger effect on the uphole refraction data than a cavity of similar size in the rock. Figure 11 shows a v-shaped depression, 10 ft (3 m) deep, in the surface of a bedrock of 18,000 ft/sec (5,500 m/sec) velocity. It is repeated for a bedrock of 6,000 ft/sec (1,800 m/sec) in Figure 12.

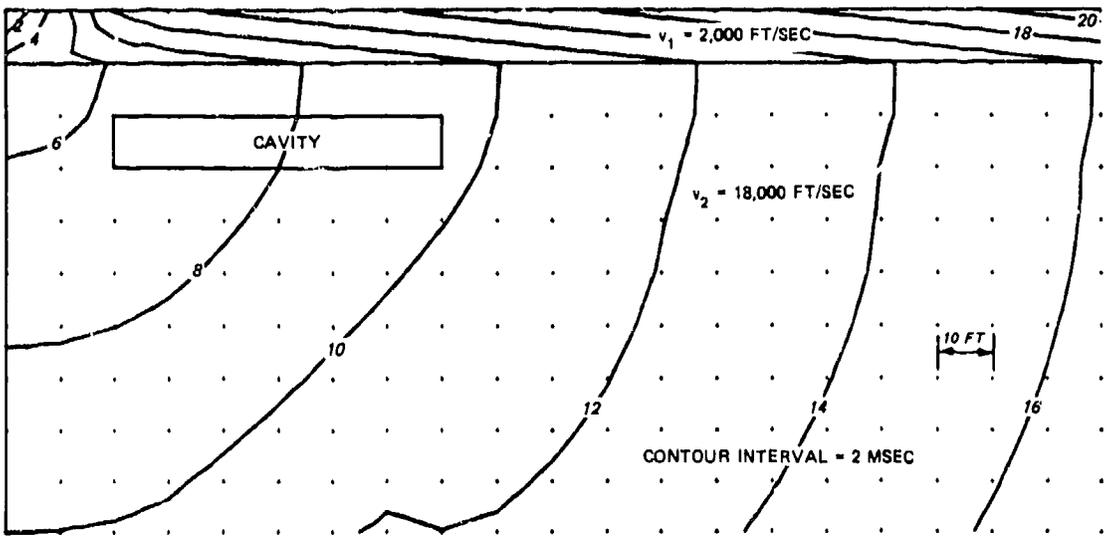

a. MEISSNER DIAGRAM

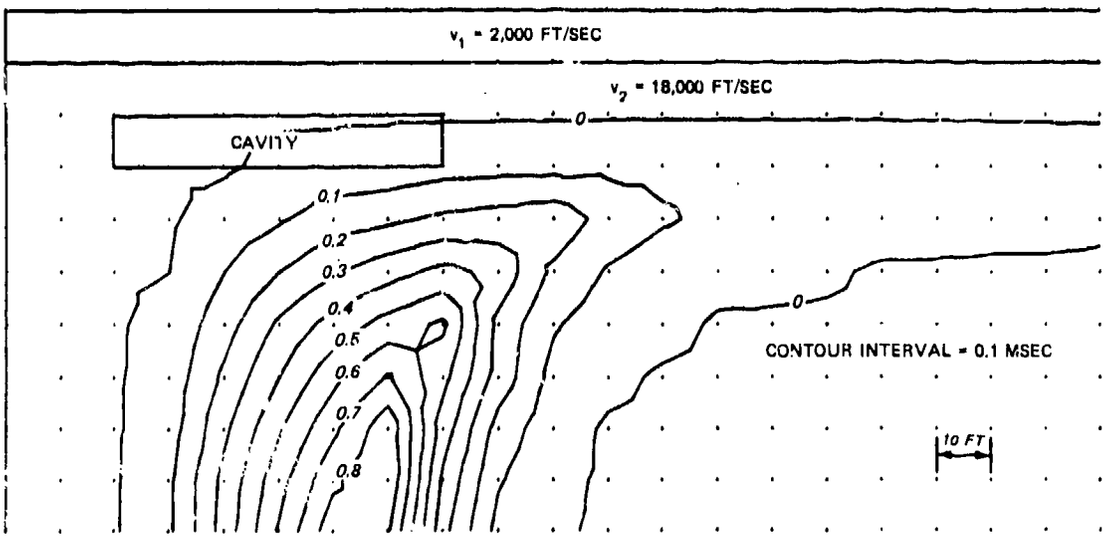

b. ANOMALY DIAGRAM

Figure 9. Meissner diagram and anomaly diagram showing effect of a 10- by 60-ft cavity in bedrock of 18,000-ft/sec compression wave velocity

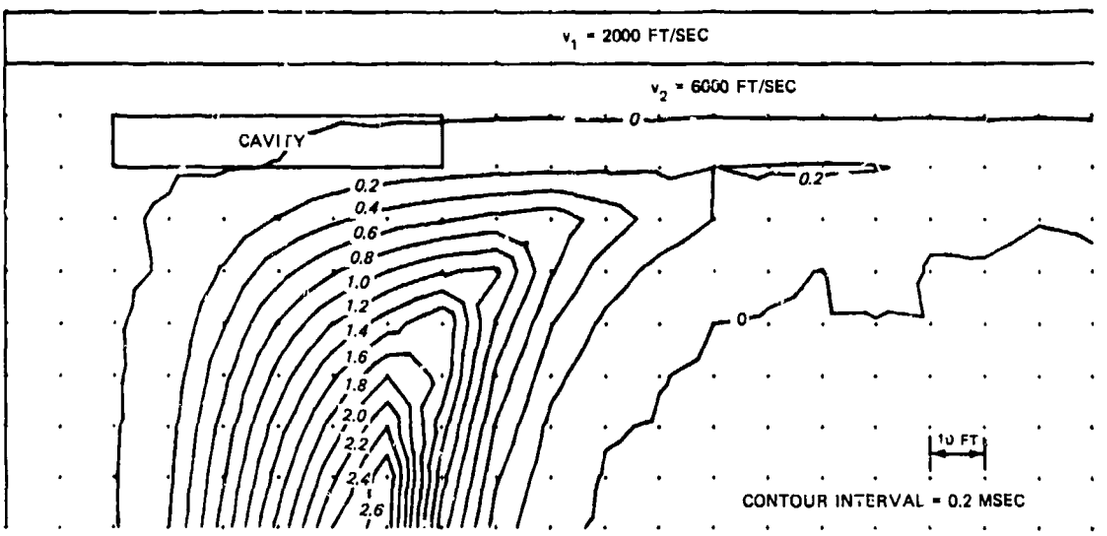

Figure 10. Anomaly diagram showing effect of 10- by 60-ft cavity in bedrock of 6000-ft/sec compression wave velocity

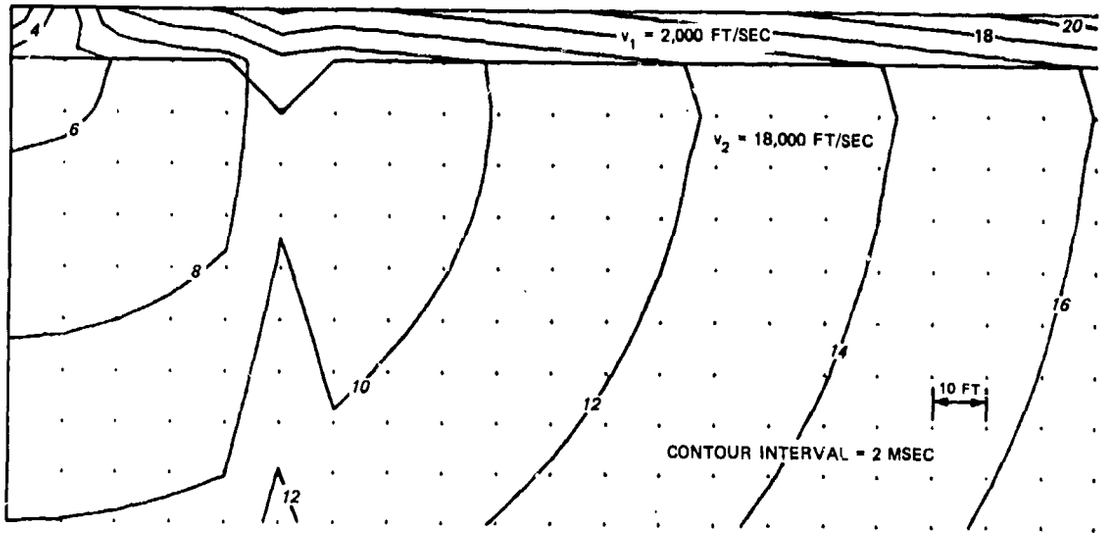

a. MEISSNER DIAGRAM

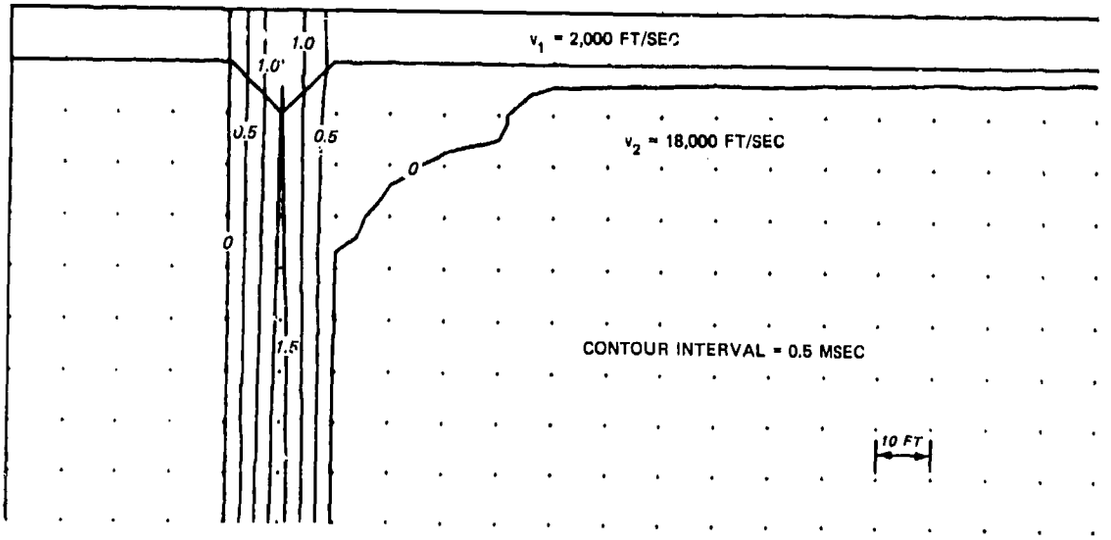

b. ANOMALY DIAGRAM

Figure 11. Meissner diagram and anomaly diagram showing effect of a 10-ft-deep, v-shaped depression in surface of 18,000-ft/sec bedrock

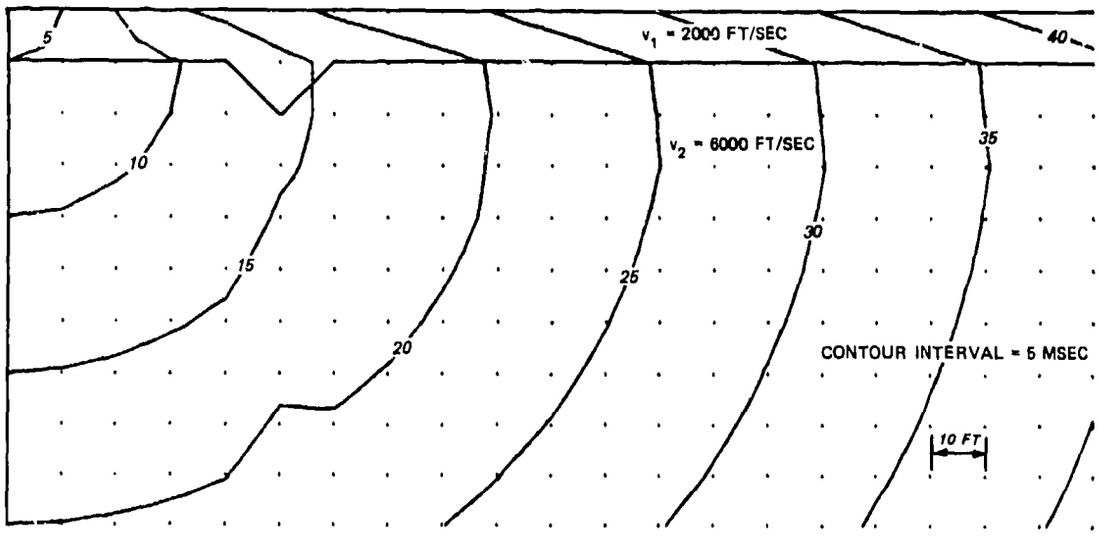

a. MEISSNER DIAGRAM

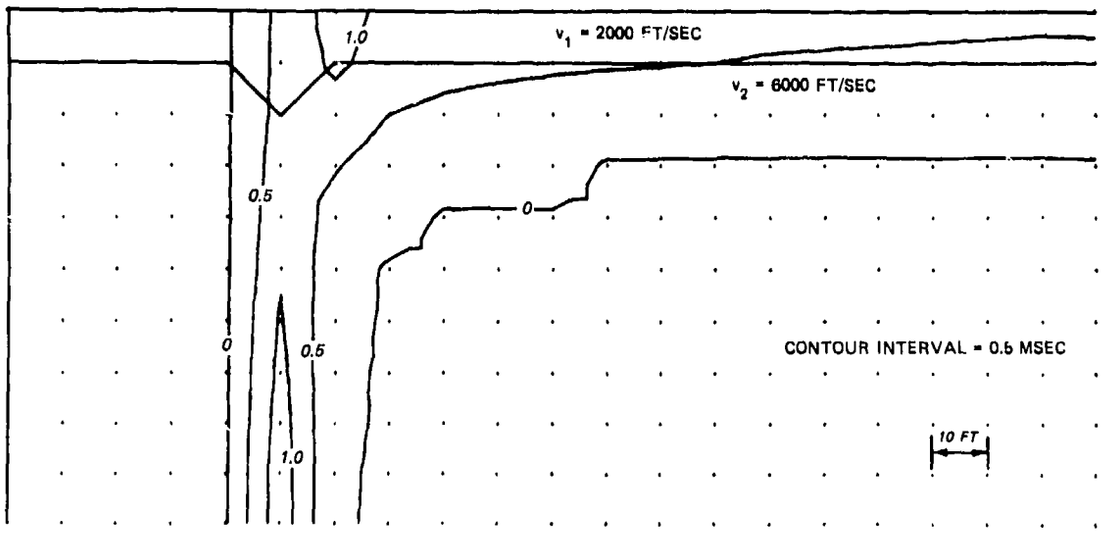

b. ANOMALY DIAGRAM

Figure 12. Meissner diagram and anomaly diagram showing effect of a 10-ft-deep, v-shaped depression in surface of 6000-ft/sec bedrock

Contrary to experience with the cavity, the time anomaly is larger in the case of the higher velocity bedrock. The anomaly diagram is notable for the pattern of strong vertical lineation that is vertically in line with the trench. Note that the anomaly is positive in sense, meaning that the trench caused longer travel times as compared with those that would have been observed without it.

28. The case of a ridge on the bedrock surface is not quite the inverse of the trench, as Figure 13 shows. The ridge shown here is a triangular wedge, 10 ft (3 m) high, on the surface of a bedrock of 6000 ft/sec (1800 m/sec). Note that the time anomaly is negative in sense and amounts to about -3.7 msec. Also, the anomaly is confined to a fairly small part of the diagram. Travel times to geophones very close to or very distant from the borehole are not affected.

Offset in bedrock surface

29. A vertical offset in the bedrock surface, such as might be caused by a vertical fault, is shown in Figures 14 and 15. The bedrock has a compression wave velocity of 6000 ft/sec (1800 m/sec) and it is overlain by soil having a velocity of 2000 ft/sec (600 m/sec). There is a 10-ft (3-m) vertical offset, or step, in the soil-rock interface. The geological conditions represented in Figures 14 and 15 are identical, but in Figure 14 the borehole, and thus the shot locations, are at the left, on the lower side of the offset, while in Figure 15 the borehole is at the right, on the higher side of the offset.

30. In Figure 14, the bedrock surface appears to be at 50-ft (15-m) depth, which is its actual depth at the borehole location. The Meissner diagram bears a strong visual resemblance to that of the ridge on the bedrock surface, as shown in Figure 13. The resemblance is superficial, however, as a comparison of the anomaly diagrams makes clear. The anomaly diagram for the offset shows a maximum value slightly greater than 4.5 msec, negative in sense, but it becomes constant at large distances from the borehole, and there is no reversal.

31. If the borehole is on the higher side of the offset, as shown in Figure 15, the apparent interface is again continuously horizontal across the Meissner diagram and is at the same level as at the borehole.

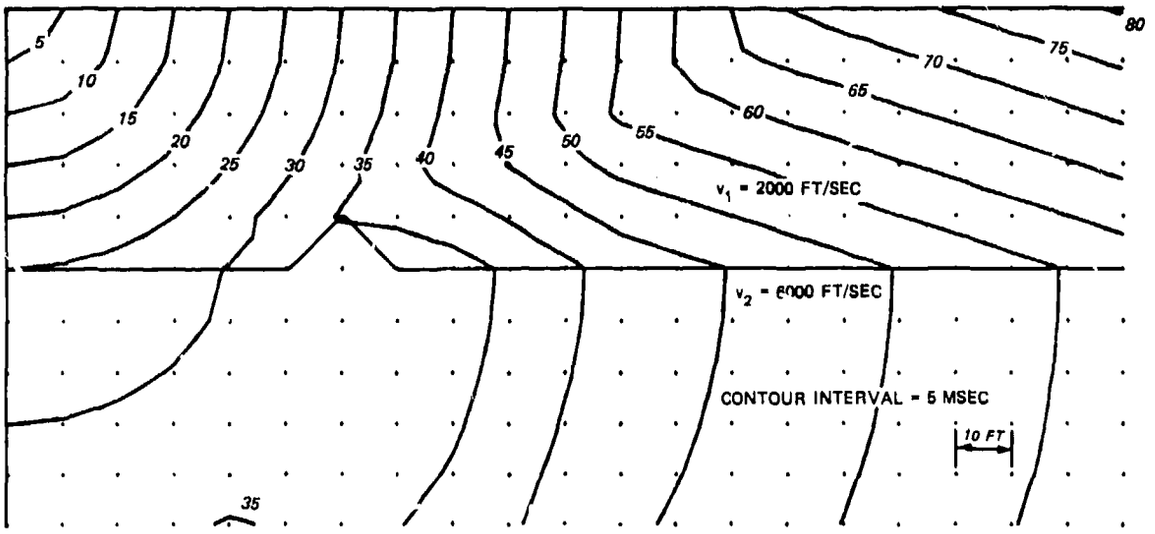

a. MEISSNER DIAGRAM

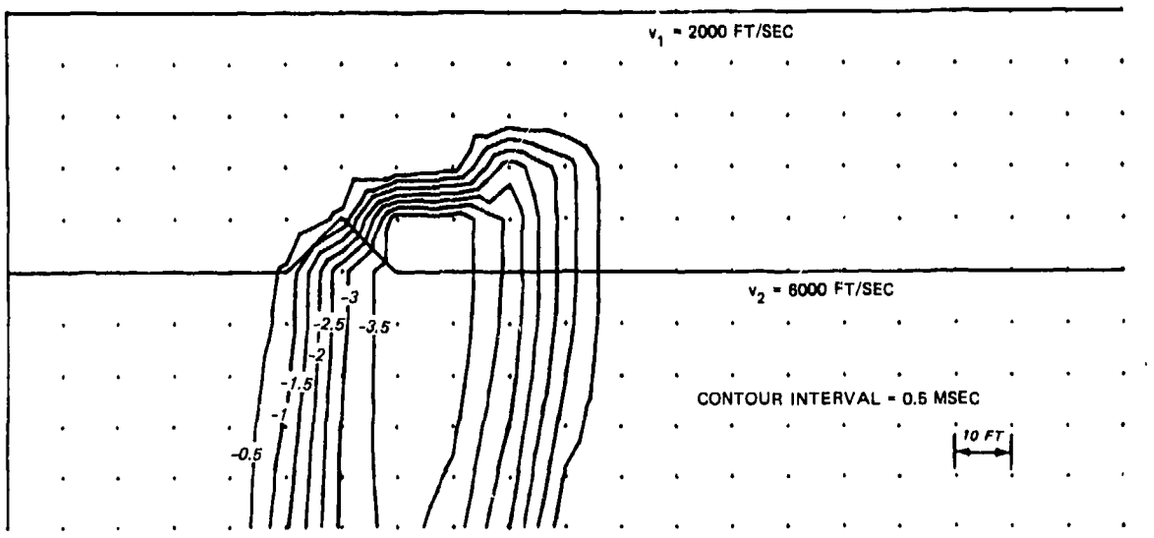

b. ANOMALY DIAGRAM

Figure 13. Meissner diagram and anomaly diagram showing the effect of a 10-ft-high ridge on the surface of a 6000-ft/sec bedrock

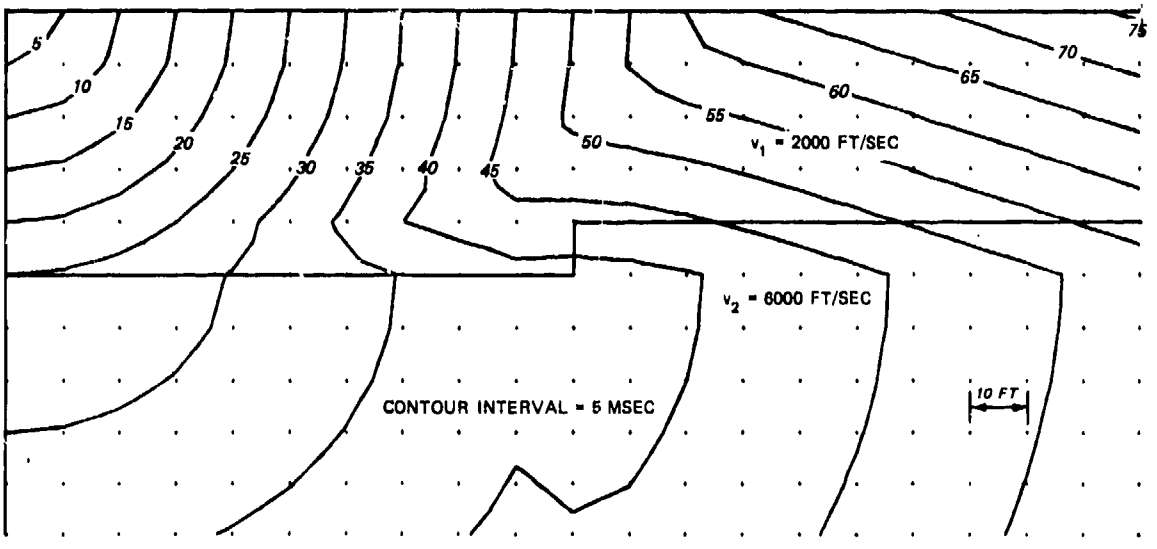

a. MEISSNER DIAGRAM

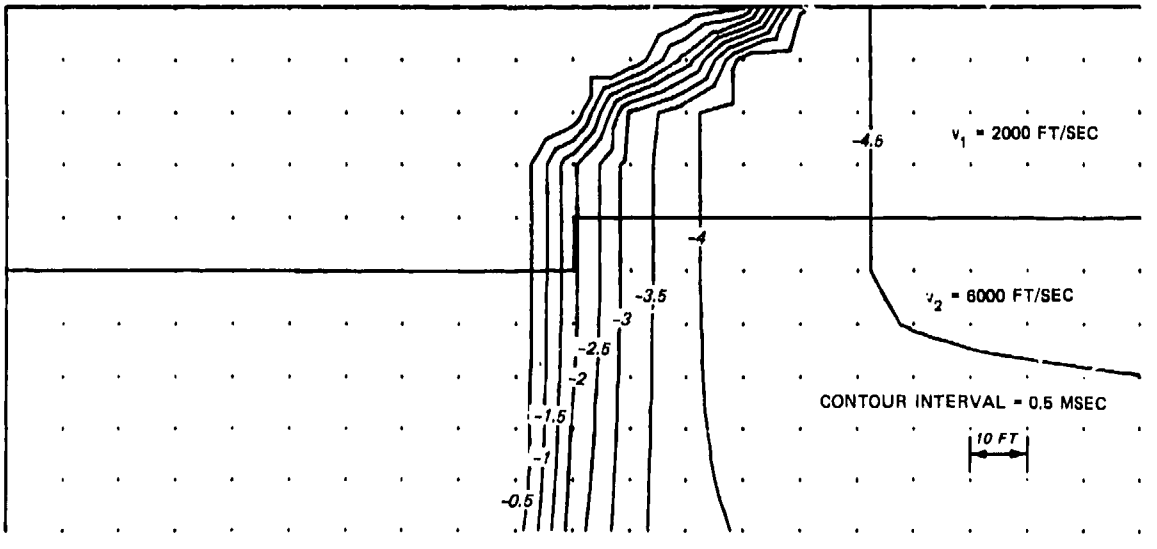

b. ANOMALY DIAGRAM

Figure 14. Meissner diagram and anomaly diagram showing the effect of a 10-ft vertical offset in the surface of a 6000-ft/sec bedrock with borehole on the lower side

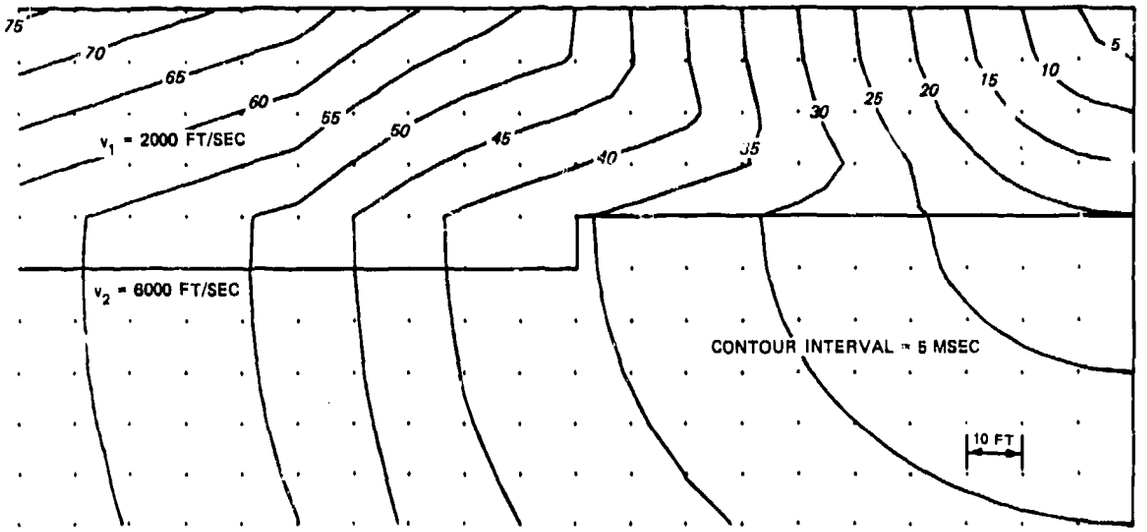

a. MEISSNER DIAGRAM

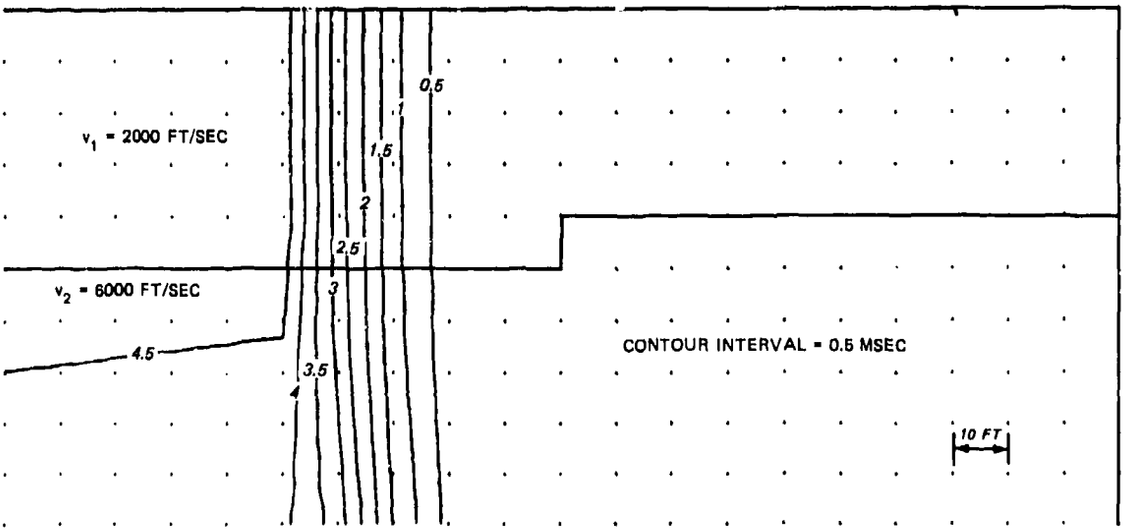

b. ANOMALY DIAGRAM

Figure 15. Meissner diagram and anomaly diagram showing the effect of a 10-ft vertical offset in the surface of a 6000-ft/sec bedrock with borehole on the higher side

The anomaly diagram is very similar to that in Figure 14, except for the part in the area of transition between the direct wave and the head wave. Also, the diagram's maximum value has the same magnitude as does the value presented in Figure 14, but the value is opposite in sign.

32. Once the geological anomaly has been recognized as an offset in the bedrock surface, its sense and approximate size can be found by trial from the sense and magnitude of the time anomaly. Once a trial value for the amount of offset has been chosen (by guess), the travel time and the time anomaly can be computed for any shot point-geophone combination in the area of the maximum anomaly. This will provide the basis for a proportional adjustment of the trial value of the offset to obtain a new trial value. Alternatively, and preferably, with a borehole at each end of the line, the amount of offset can be seen immediately from the difference in the two apparent depths to the interface.

33. An estimate of the horizontal position of the offset can be made from consideration of the ray paths. Considering the shot point nearest the intersection of the bedrock surface and the borehole, one can see that if the borehole is on the lower side of the offset, the first geophone at which the travel time is affected is, at most, the first one beyond the offset. This is because the travel time for a signal propagated vertically or nearly vertically from the edge of the offset is smaller than for the signal refracted from the deeper bedrock. The ray path for the refracted signal leaves the bedrock surface at a horizontal distance $H_1 \tan \theta_c$ from the geophone, where H_1 is the depth to the bedrock and θ_c is the critical angle of refraction. If the borehole is on the higher side, the situation is reversed, and the nearest affected geophone is the first one beyond a distance $H_1 \tan \theta_c$ from the offset.

Dipping strata

34. Figures 16 and 17 illustrate a case in which the soil-bedrock interface has a dip component along the line of survey of 30 vertical in 200 horizontal. The velocities used are the same as in the earlier example. In Figure 16, the top of the bedrock is at 50 ft (15 m) in the

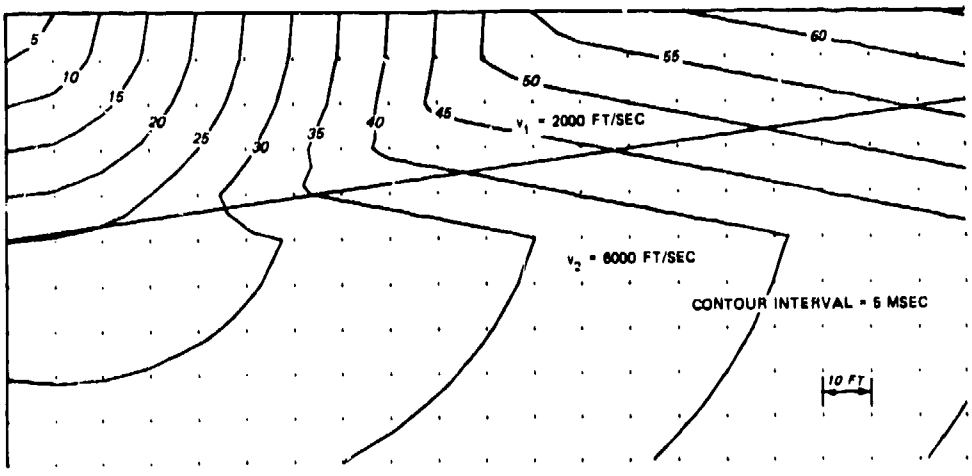

a. MEISSNER DIAGRAM

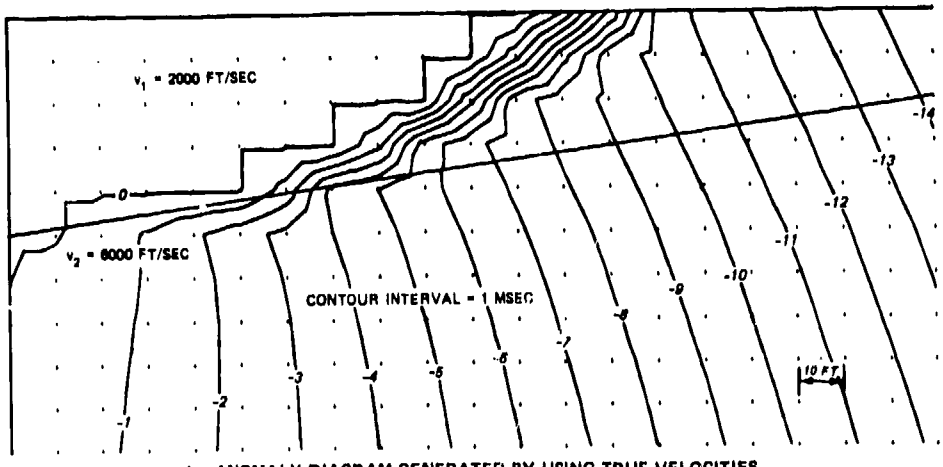

b. ANOMALY DIAGRAM GENERATED BY USING TRUE VELOCITIES, v_1 = 2000 FT/SEC, v_2 = 6000 FT/SEC

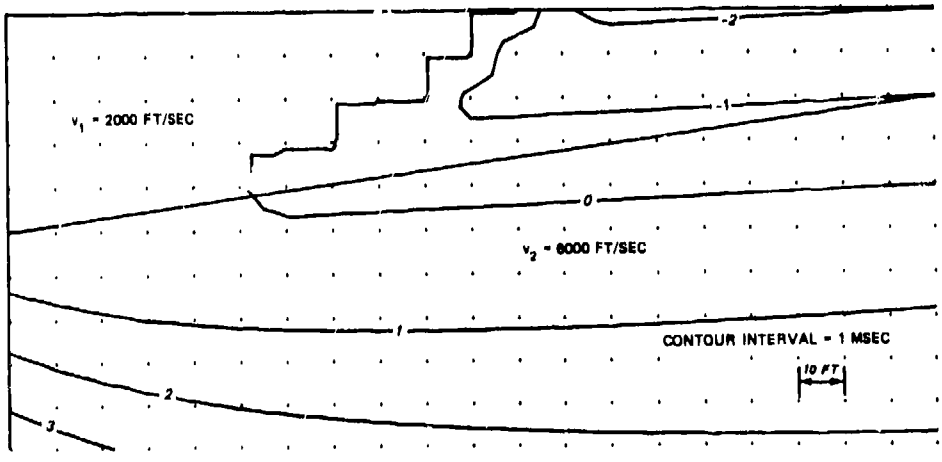

c. ANOMALY DIAGRAM GENERATED BY USING APPARENT VELOCITIES, v_1 = 2,000 FT/SEC, v_2 = 10,800 FT/SEC

Figure 16. Meissner diagram and anomaly diagrams showing effect of dipping strata, with borehole at the downdip end of the seismic line

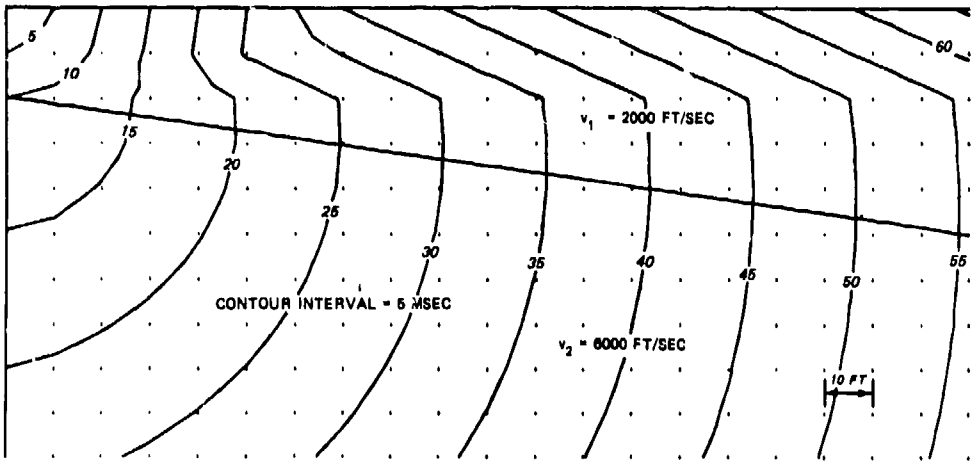

a. MEISSNER DIAGRAM

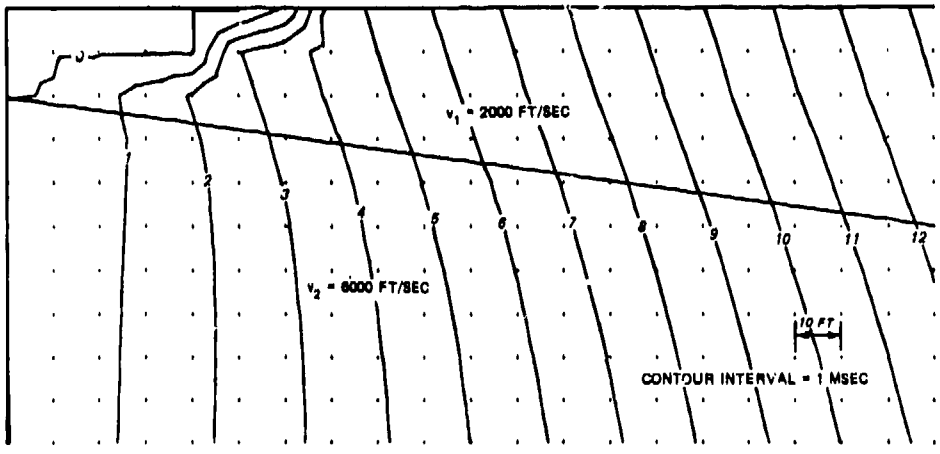

b. ANOMALY DIAGRAM GENERATED BY USING TRUE VELOCITIES, v_1 = 2000 FT/SEC, v_2 = 6000 FT/SEC

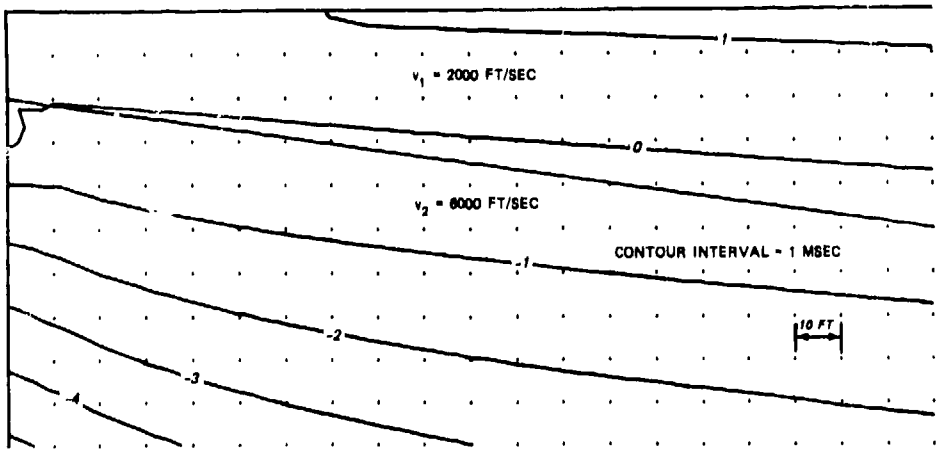

c. ANOMALY DIAGRAM GENERATED BY USING APPARENT VELOCITIES, v_1 = 2000 FT/SEC, v_2 = 4300 FT/SEC

Figure 17. Meissner diagram and anomaly diagrams showing effect of dipping strata, with borehole at the updip end of the seismic line

borehole, and the dip is up away from the borehole. The apparent soil-rock interface in the Meissner diagram is horizontal and is at the same depth as in the borehole. The Meissner diagram is visually similar to that for a horizontal bedrock surface. The visible differences are relatively subtle and likely would be concealed by the noise that would be present in real field data. The compression wave velocity of the soil layer, 2000 ft/sec (600 m/sec), is measured without difficulty from the diagram. The compression wave velocity of the bedrock layer, however, is less clear. A measurement made along the borehole axis in the diagram yields a velocity of 6000 ft/sec (1800 m/sec), which is the true velocity of the medium. Figure 16b shows the anomaly diagram that results from this interpretation. Alternatively, the velocity might be interpreted from the horizontal spacing between the head wave positions, to get the same apparent velocity that would be obtained in a surface refraction survey. This yields an apparent velocity of 10,800 ft/sec (330 m/sec). The anomaly diagram resulting from this interpretation is shown in Figure 16c.

35. Figure 17 shows the results that would be obtained with the borehole at the opposite end of the survey line. It is shown with the borehole at the left, with the bedrock at a 20-ft (6-m) depth in the borehole, and with the soil-rock interface dipping away from the borehole. The Meissner diagram again bears a close visual resemblance to that for a horizontal interface, and the apparent interface in the diagram is horizontal and at the same level as in the borehole. The apparent velocity, as measured at the apparent interface or between head wave positions, is about 4300 ft/sec (1300 m/sec), while the true velocity can be measured along the axis of the borehole. The anomaly diagrams resemble those in Figure 16, but show a reversal in the sense of the anomaly.

36. The existence of dipping strata can be readily recognized if the uphole refraction survey is carried out with a borehole at each end of the line, to yield complementary Meissner diagrams such as in Figures 16 and 17. The difference of elevation of the refracting layer at the two boreholes will be directly evident from the boring logs, and the

Meissner diagram will permit discrimination between an abrupt offset and a continuous dip. The dip can also be readily recognized and measured by running forward and reversed surface refraction surveys along the same line. Where the uphole refraction survey is limited to a single borehole, this should be done to provide the needed supplementary information.

Errors in measurement and interpretation

37. Measurement errors. Figure 18a shows a Meissner diagram for a simple case of 3 horizontal layers, and Figure 18b shows the diagram resulting after a normally distributed random error with a standard deviation of 0.5 msec was applied to the arrival times. Finally, Figure 18c shows the anomaly diagram, on which those random errors are contoured. Figure 18b, which resembles a Meissner diagram obtained from real field data, illustrates the point that the normal noise due to inhomogeneities in the materials and to errors of measurement tends to obscure the finer or more subtle features of the Meissner diagram, so that such subtle features cannot generally be relied on for interpretation. The anomaly diagram, which represents a reasonably realistic error level with a standard deviation of 0.5 msec, shows a formless pattern that can be taken, when it is achieved in an anomaly diagram, as a signal that all significant geological conditions have been accounted for in the interpretation.

38. Resolution of layer boundaries. The spatial resolution of geological features is naturally limited by the fineness of the grid on which data are obtained. The foregoing diagrams all show, for simplicity's sake, strata boundaries that coincide with shot point depths, but in the field such a coincidence will be the exception. Figure 19 shows a case in which the soil overburden is 14 ft (4.3 m) thick, but the shot points are at 10-ft (3-m) intervals. The mechanical contouring yields a diagram on which a 10-ft- (3-m-) thick layer of intermediate velocity is shown in the interval between the shot points at 10 and 20 ft (3 and 6 m). In fact, the data are wholly consistent with the existence of such a layer, but in interpretation its existence would be denied in favor of the simplest set of geological conditions that can

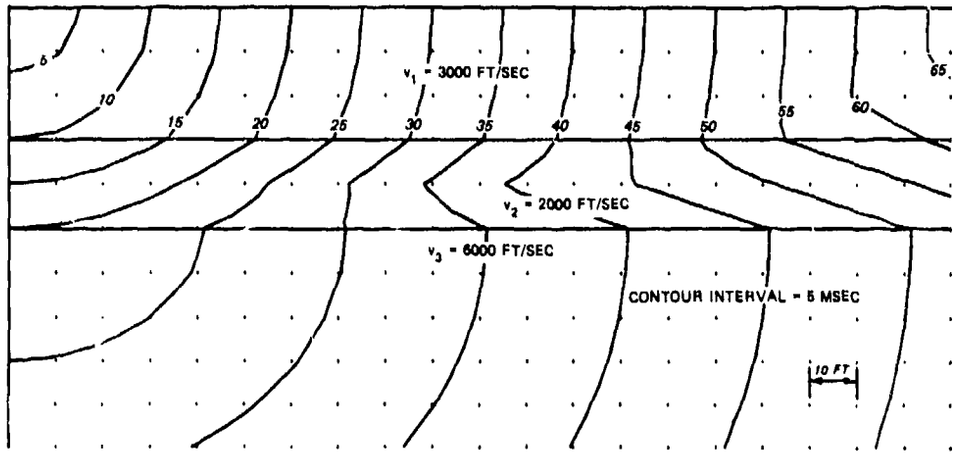

a. MEISSNER DIAGRAM

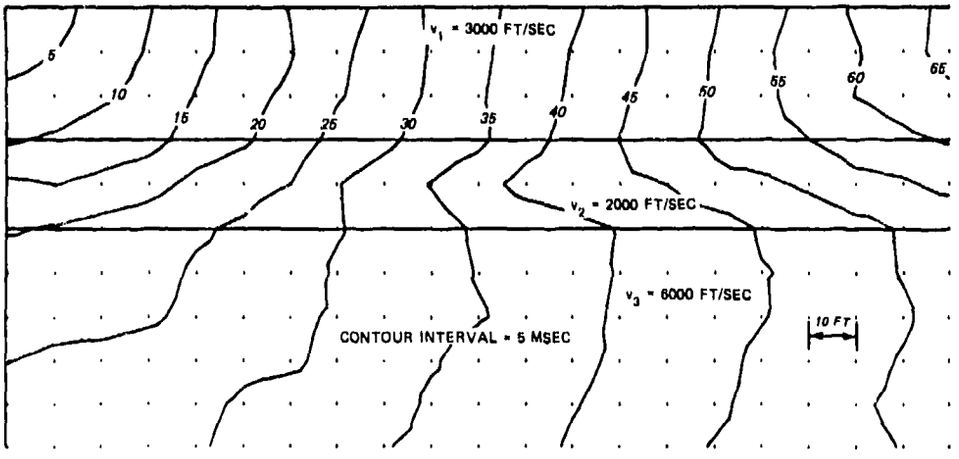

b. MEISSNER DIAGRAM WITH EFFECTS OF RANDOM ERRORS

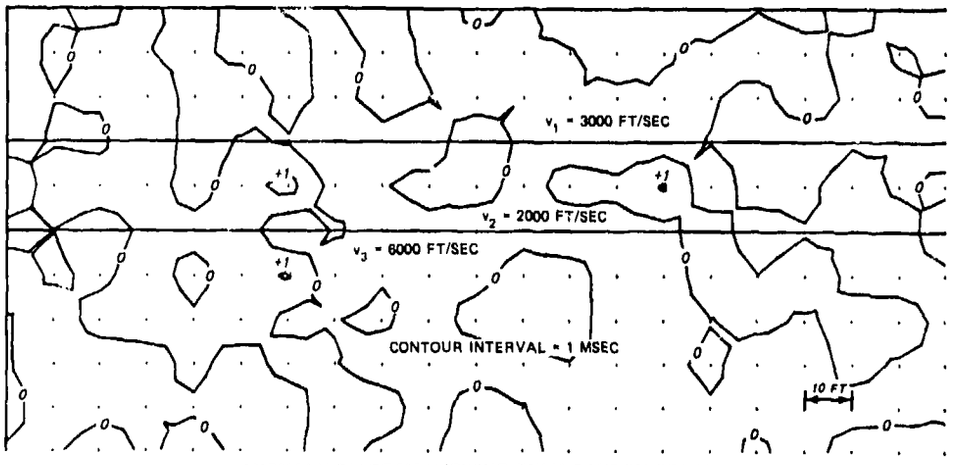

c. ANOMALY DIAGRAM SHOWING ONLY RANDOM ERRORS

Figure 18. Meissner diagrams and anomaly diagram showing the effects of random errors

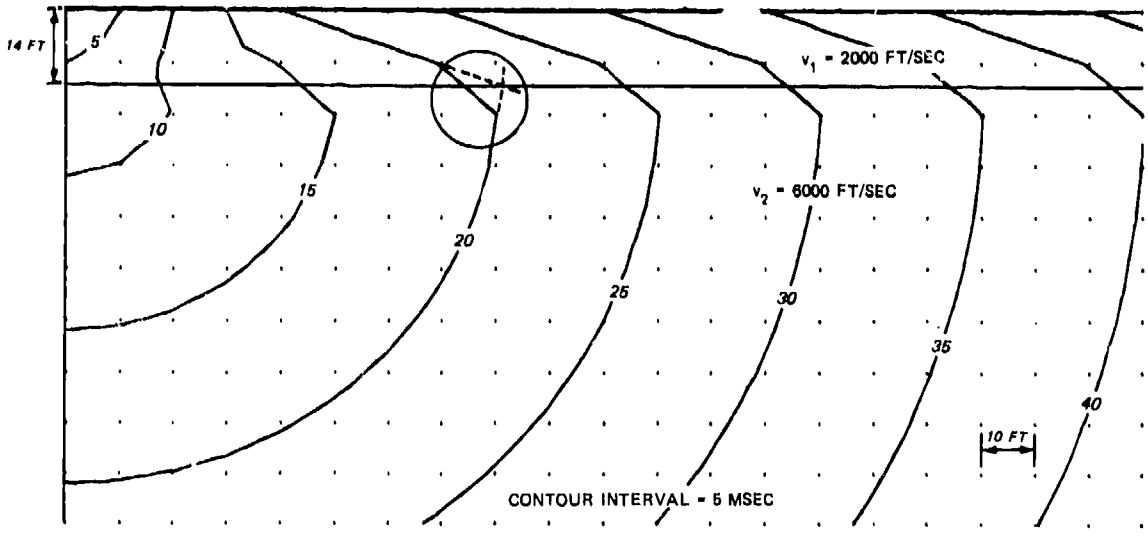

Figure 19. Interpolation of layer boundary on the Meissner diagram

be made to fit the data and is otherwise geologically reasonable. This leads to the choice of a boundary within the interval, and its location is found, as shown in Figure 19, by simply projecting the contours from above and below to find their intersection.

39. Errors in interpretation of velocity. In addition to helping in the identification of the nature of geological anomalies, the anomaly diagram can be useful as an aid in interpretation even in uncomplicated situations. For example, the anomaly diagram shown in Figure 20 is the result of an erroneously high choice of the surface layer velocity from a Meissner diagram for a simple two-layer system. Since the interpreted velocity was on the high side, the time anomaly is positive in sign.

40. In the example shown, the surface layer velocity, 2000 ft/sec (600 m/sec), was erroneously interpreted as 2500 ft/sec (760 m/sec), which implies a travel time of 0.4 msec/ft (1.3 msec/m). By scaling the distance between contours in the primary wave region of the anomaly diagram (as opposed to the head wave region), one finds the travel time anomaly, or residual travel time, to be 0.1 msec/ft (0.33 msec/m). Thus the correct travel time is 0.5 msec/ft (1.64 msec/m), and its reciprocal is 2000 ft/sec (600 m/sec), the correct velocity.

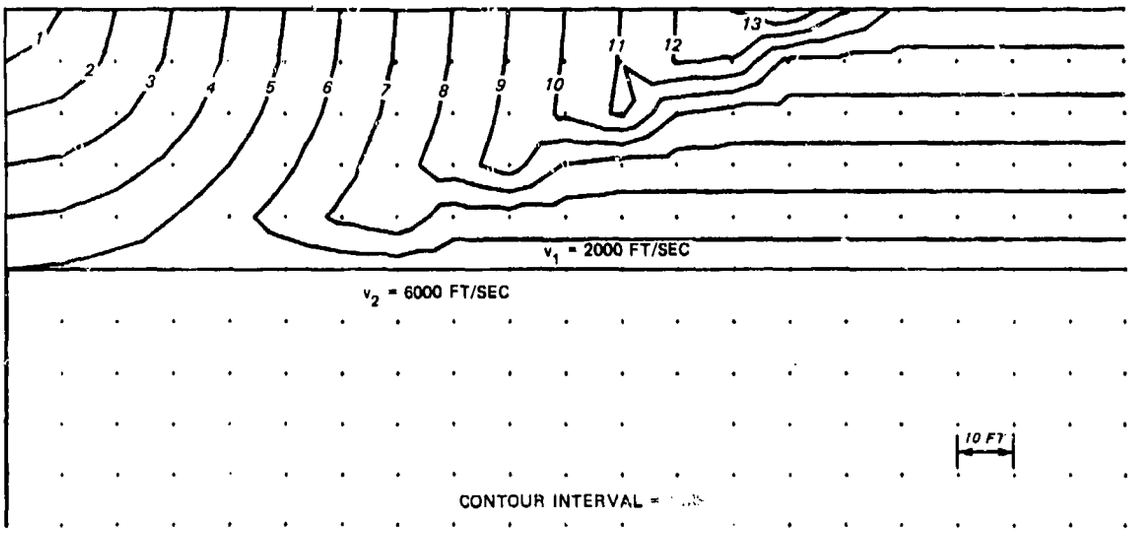

Figure 20. Anomaly diagram resulting from erroneously high determination of surface layer velocity

41. Figure 21 shows the anomaly diagram for the same set of geological conditions, obtained by too high a choice of the bedrock velocity. The correction can be made in the same manner as described above.

42. Errors in location of layer boundaries. Figure 22 shows the anomaly diagram occurring as a consequence of an error of 10 ft (3 m) in the choice of the depth of the soil-rock interface. The form of the anomaly is clear and simple: a concentration of horizontal contours in the interval between the interpreted depth of the horizon and the correct depth. The size of the time anomaly, and the contour density, depends on the size of the depth error and the degree of velocity contrast between the two layers. A band of contours also occurs in the zone of transition between the direct wave and the head wave in the soil layer, but the general absence of contours elsewhere indicates that the velocities were correctly chosen.

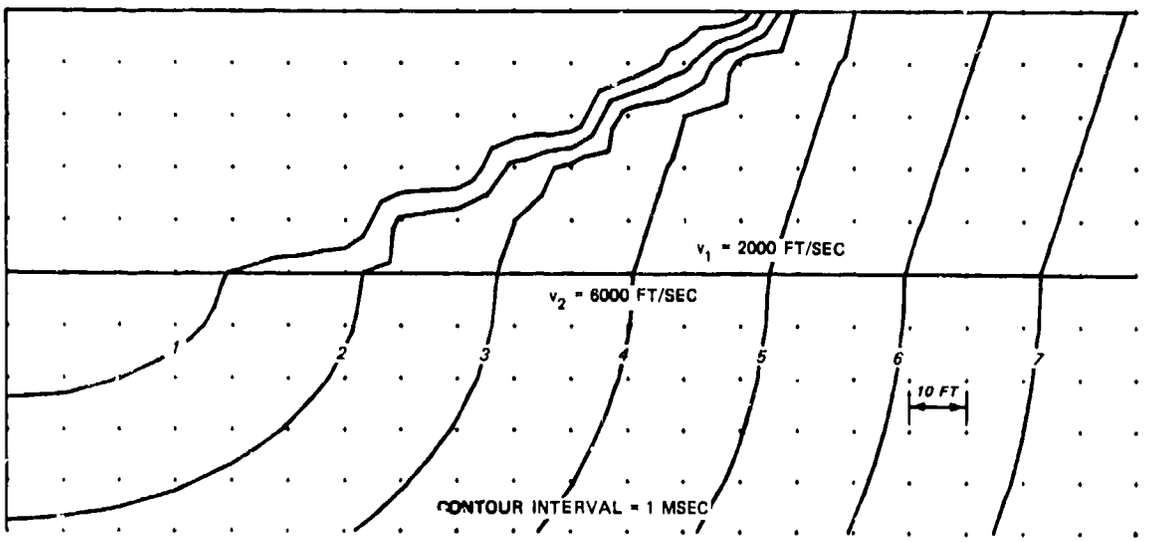

Figure 21. Anomaly diagram resulting from erroneously high determination of second layer velocity

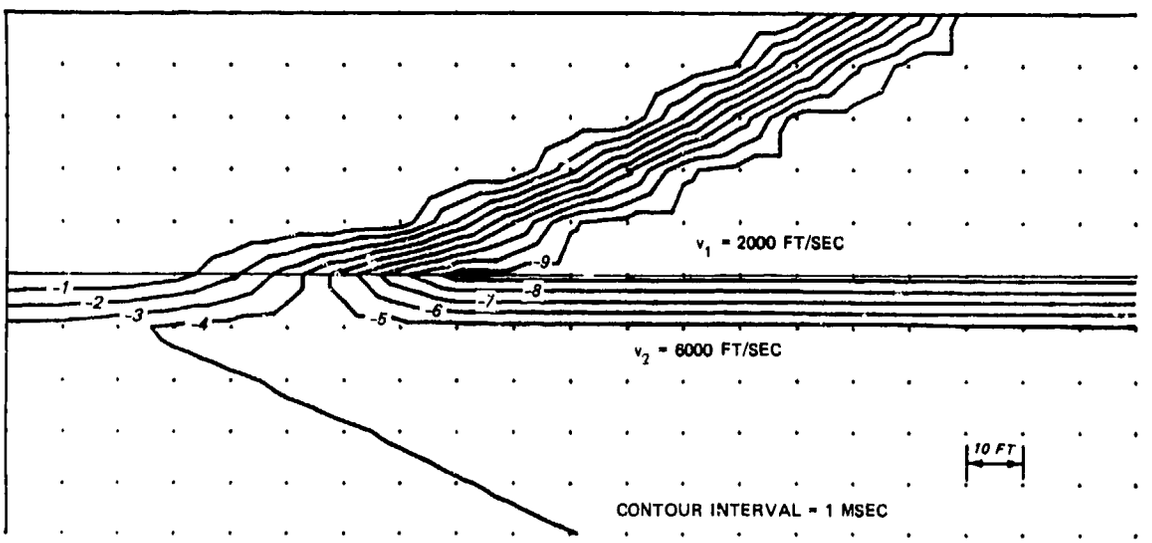

Figure 22. Anomaly diagram resulting from erroneous determination of depth of second layer surface

PART IV: EXAMPLES OF FIELD DATA

Arizona Site

43. An uphole refraction survey was performed as a part of the geotechnical investigation for the MISERS BLUFF II high-explosive test events at Planet Ranch, Ariz. during 1978 (Jackson, Ballard, and Phillips 1979). The survey was carried out on 350-ft (107-m) east-west line with a borehole at each end (borings WES 2 and WES 3, at the east and west ends, respectively). Three additional borings (WES 4, WES 5, and WES 6) were made subsequently along the line. Meissner diagrams and anomaly diagrams for this survey are shown in Figures 23 and 24.

44. The Meissner diagram in Figure 23a is drawn on data obtained from shots in boring WES 3, at the west end of the line. The apparent layer boundaries as interpreted from this diagram are at 50 and 150 ft (15 and 46 m), and the velocities are 1,260 ft/sec (384 m/sec), 4,900 ft/sec (1,500 m/sec), and 13,000 ft/sec (4,000 m/sec), from top to bottom. The anomaly diagram drawn from the data on the basis of this set of layer parameters is shown in Figure 23b. The Meissner diagram and anomaly diagram for the survey from WES 2 are shown in Figure 24. The same velocities were used in this case, but the apparent depth of the bottom layer was taken as 123 ft (37.5 m). The contours extend only to a distance of 5 ft (1.5 m) from the ground surface and to 10 ft (3 m) from the boreholes because the shallowest shot and the nearest geophone were at those respective distances.

45. The soil profile consists of granular alluvium of varying thickness, overlying conglomeratic sandstone. The change in velocity at 50 ft (15 m) clearly represents the ground water table within the alluvium, and the 13,000-ft/sec (4,000-m/sec) layer represents the sandstone bedrock. The configuration of the bedrock surface has been interpreted with the use of depths obtained in the five borings and the results of the seismic survey, and is shown with a hachured line. Comparison of Figure 23 with Figure 14, and of Figure 24 with Figure 15, strongly suggests the presence of an offset in the bedrock surface near

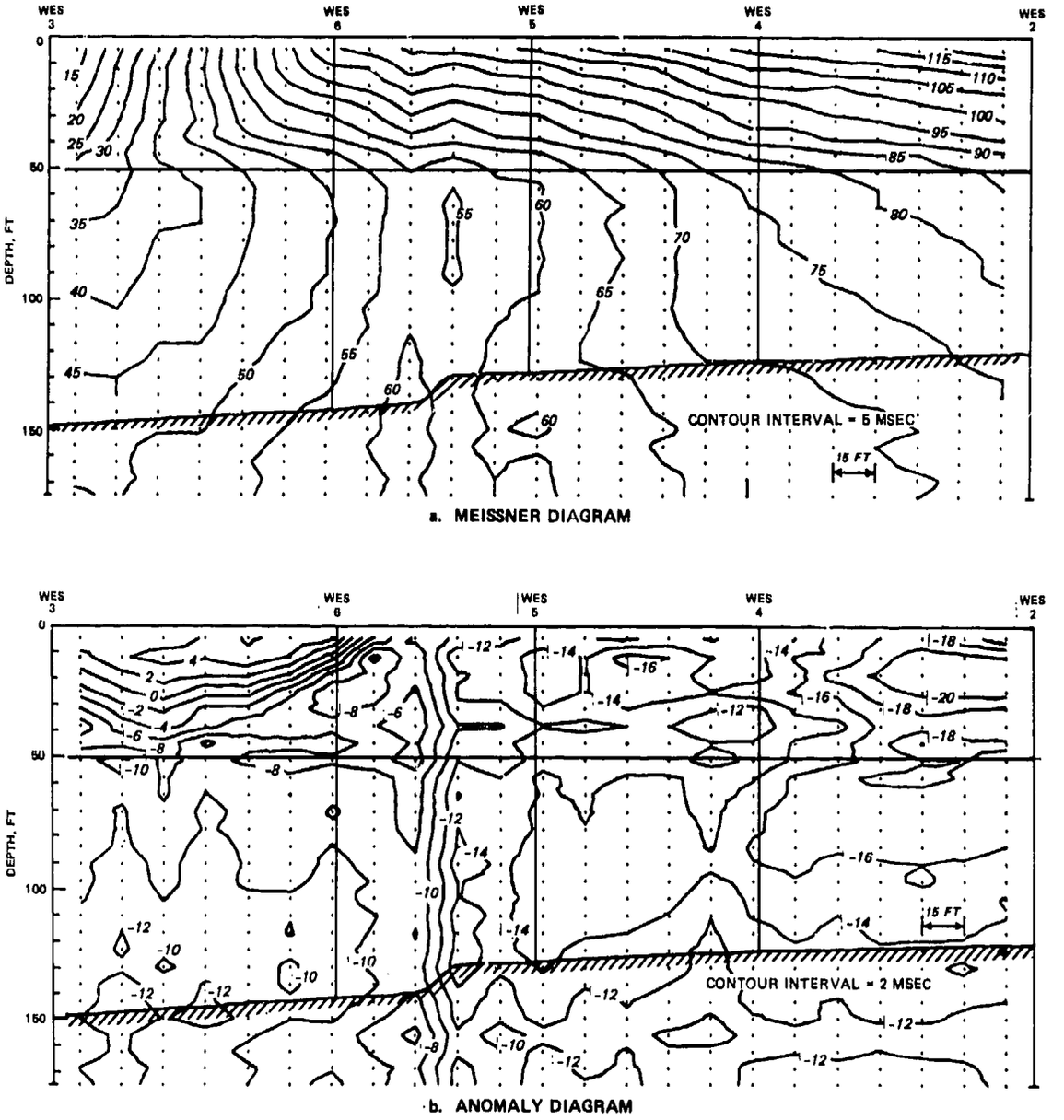

Figure 23. Uphole refraction survey from boring WES 3 toward WES 2, Planet Ranch, Ariz.

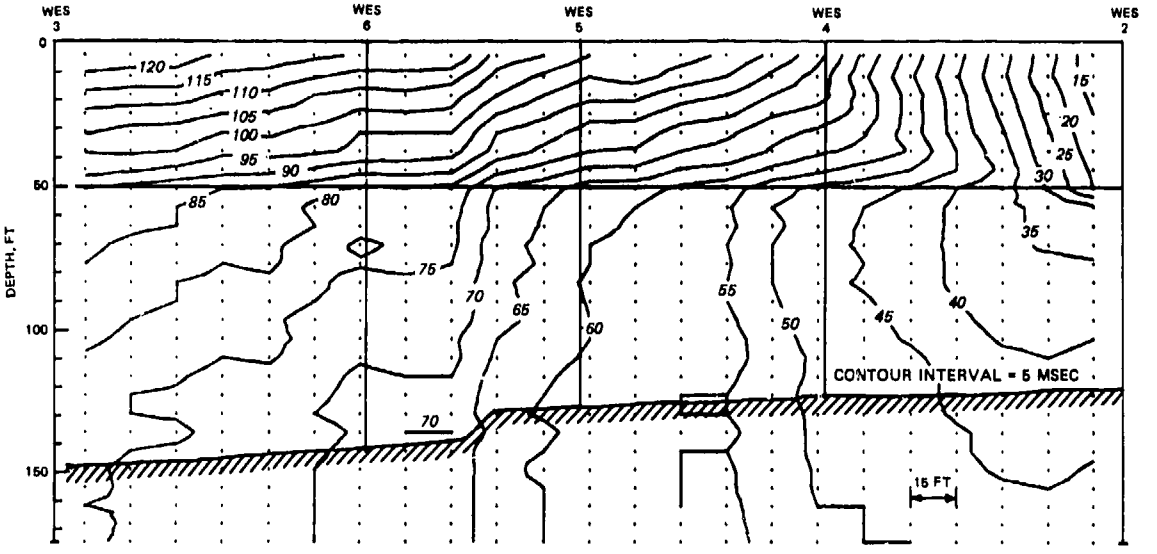

a. MEISSNER DIAGRAM

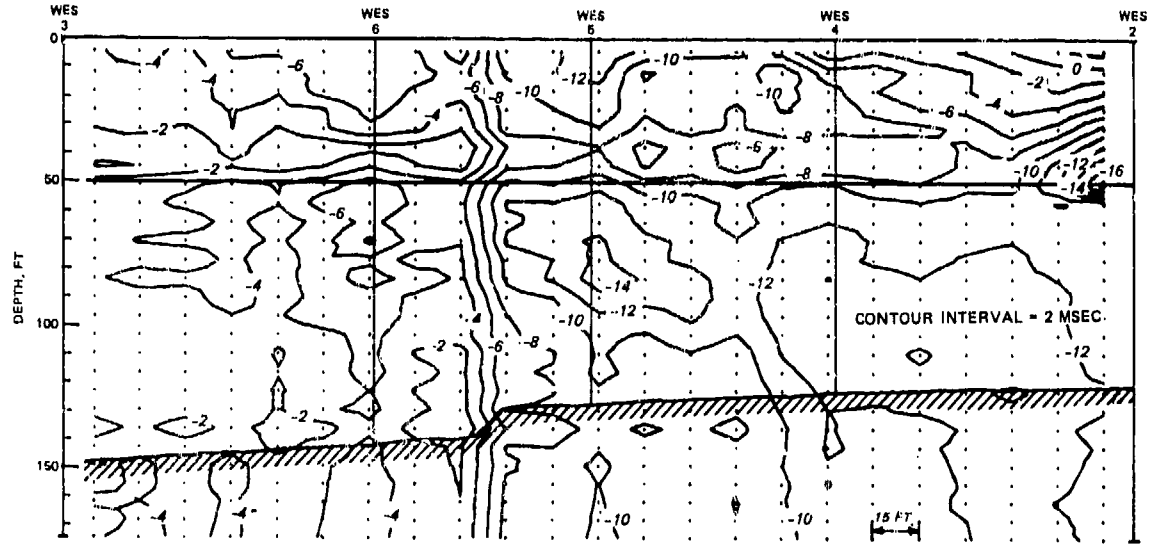

b. ANOMALY DIAGRAM

Figure 24. Uphole refraction survey from boring WES 2 toward WES 3, Planet Ranch, Ariz.

the middle of the line, and this is further suggested by a drop of the bedrock surface from 127 ft (38.7 m) in WES 5 to 141 ft (43 m) in WES 6, which indicates a steeper average gradient than elsewhere in the cross section. Accordingly, the surface is drawn with a steep offset midway between WES 5 and WES 6.

46. It is noteworthy that in the band of vertically oriented contours, which is interpreted as representing an offset in the bedrock surface, the values of the contours are negative in both anomaly diagrams. These values depend upon the accuracy of the choice of the layer velocities and the depths to the layer boundaries, as well as upon soil inhomogeneities and departures of the geometry from the ideal horizontal stratification. It is the local relative value and gradient of the anomaly, which is consistent in the two anomaly diagrams, that is indicative of the nature of the geological anomaly.

47. The boring data indicate that in addition to having an offset, the bedrock surface has an east-to-west dip that amounts to about 3 percent from WES 2 to WES 5 and about 7 percent from WES 6 to WES 3. This dip is evidently too slight to have a material effect on the anomaly diagram, since no distinct anomaly pattern such as those of Figures 16 and 17 is distinguishable above the error level.

48. There is an additional area of anomaly that is noteworthy--the concentration of contours in both anomaly diagrams in the neighborhood of the respective boreholes in the surface layer. From the spacing of the contours, it appears there is a slight difference in the apparent velocity of the surface layer in the two surveys, indicating some lateral inhomogeneity of the soil. A stronger contribution to the anomaly appears to be a higher velocity in t surface layer along the borehole than along the ground surface, as interpreted from the strong negative time anomaly from the ground surface down to the bottom of the surface layer. The borings were made with drilling mud and were subsequently cased with plastic pipe and grouted in place. At the time of shooting, the casing was filled with water to a depth of approximately 30 ft (9 m) from the surface. The higher velocity along the borehole can be explained by preferred transmission of the signal

through the water column in the casing, the grout column, and possibly a zone of mud-filled washouts or mud-invaded soil surrounding the borehole.

Waterways Experiment Station Site

49. At the proving ground of the U. S. Army Engineer Waterways Experiment Station, Vicksburg, Miss., there is a plot containing several lengths of polyvinyl chloride (PVC) pipe, with capped ends, and with various diameters up to 4 ft (1.2 m), buried at various depths in the loessial soil of the site for the purpose of studying the effectiveness of various geophysical tools in exploring for buried cavities (Butler and Murphy 1980). As a part of the investigations at this site, an uphole refraction survey was run from a borehole identified as the east borehole over a section containing a length of 4-ft- (1.2-m-) diameter pipe at a depth of 20 ft (6 m), so that the line of survey was perpendicular to the axis of the pipe. For comparison, a second line (the west borehole line) was run with similar shot point depths and geophone spacings at a nearby location where the original ground conditions were apparently similar, but without a cavity. The pipe has a surface connection so that it can be filled with water or pumped dry. It was dry at the time of these trials.

50. The plots obtained from these surveys are shown in Figure 25. In this case, the anomaly diagram represents a variation on the procedure described earlier. Since the data from a survey over similar, but virgin, ground was available, the anomaly diagram was generated by using the differences in the seismic transit times from the two surveys, thus avoiding the need to estimate layer parameters and compute times for the layered system.

51. A rough calculation of the comparative seismic travel times through virgin ground and around a 4-ft (1.2-m) empty cavity indicates that the time anomaly to be expected approximates 0.05 msec. An anomaly of this magnitude is far below the threshold of detectability, and thus no visible expression of it is expected. However, the anomaly diagram

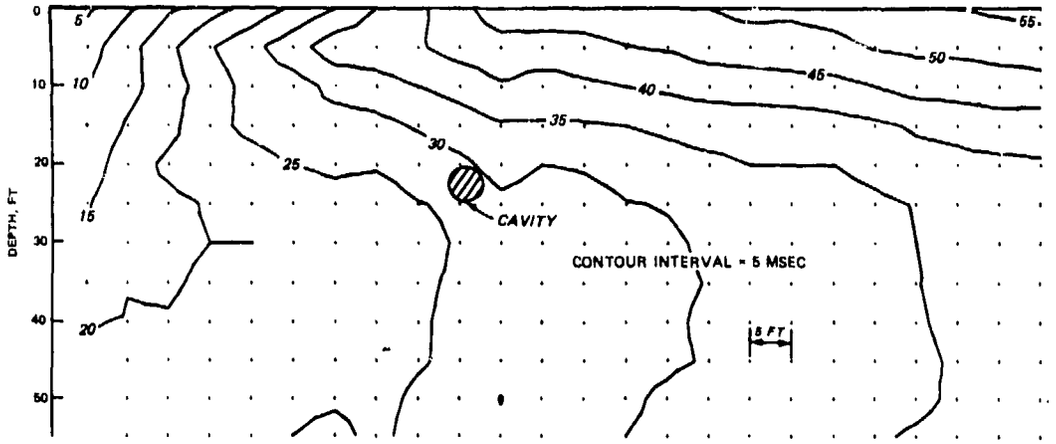

a. MEISSNER DIAGRAM FOR SURVEY AT EAST BOREHOLE

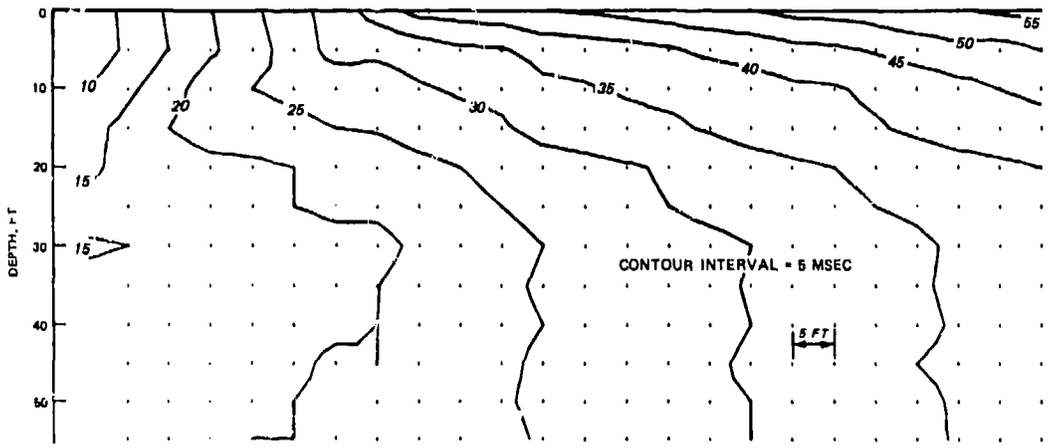

b. MEISSNER DIAGRAM FOR SURVEY AT WEST BOREHOLE

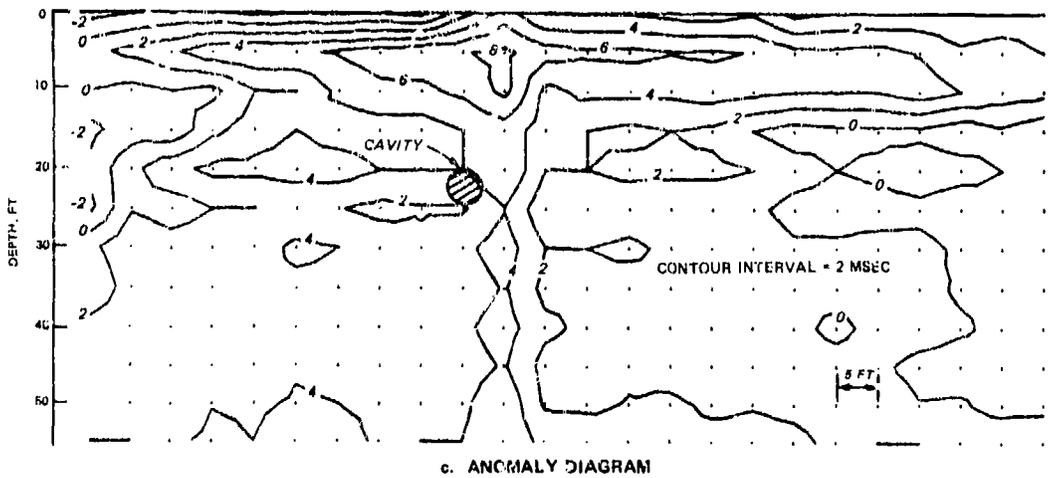

c. ANOMALY DIAGRAM

Figure 25. Uphole refraction survey at Waterways Experiment Station site; anomaly diagram (c) obtained as the differences in arrival times between the surveys at east borehole (a) and west borehole (b)

has a fairly well-defined, vertically oriented anomaly in the neighborhood of the cavity, with a magnitude of approximately 6 msec. This anomaly is presumably due to the disturbance and diminished compression wave velocity of the soil that has been backfilled in the trench in which the pipe was placed. Comparison of this anomaly diagram with those in Figures 11 and 12 also suggests an anomaly of this type.

PART V: SUMMARY AND CONCLUSIONS

Summary

52. In an uphole refraction survey, a series of shots at various depths in a single borehole is used with a line of surface geophones extending away from the hole. The first-arrival times for such a survey can conveniently be plotted on a diagram of the vertical plane through the borehole and the line of geophones, with the time for each shot point-geophone combination at a grid point vertically below the geophone and at the same elevation as the shot point. Equal-time contours drawn on the diagram represent instantaneous wave-front positions for a single fictitious shot at the top of the boring, provided that the ground consists solely of either vertically or horizontally oriented strata. In conditions other than the simply stratified case, the wave-front diagram for a shot at the ground surface is not the same as the diagram of contours drawn on uphole refraction data, and so to preserve the distinction the term "Meissner diagram" after R. Meissner (1961) is used in this report for the latter.

53. In most cases, a partial interpretation of the Meissner diagram can be made on the basis of the wave-front analogy to yield an estimate of the layer velocities and the locations of the layer boundaries. However, anomalies should not be interpreted on the basis of wave-front behavior because it is in those areas that the wave-front analogy most seriously breaks down. Also, the area of the anomaly in a Meissner diagram does not generally coincide with the location of the geological feature that is responsible for it.

54. A systematic approach to the interpretation of the Meissner diagram is proposed in this report. Its first step is the determination of a tentative set of layer parameters (velocities and thicknesses) on the basis of the wave-front interpretation. Theoretical seismic travel times for the uphole refraction survey are then computed for a simple layered system with these parameters, and an anomaly diagram is

generated by drawing contours on the differences between the observed and theoretical times. The nature of many geological features may be identifiable by comparison of anomaly diagrams obtained from field data with anomaly diagrams representing known or hypothesized geological conditions. The procedure can be iterated by computing theoretical travel times for the interpreted conditions to yield second and later generations of anomaly diagrams.

55. Meissner diagrams and their companion anomaly diagrams have been presented for cases of buried cavities, ridges and depressions on a bedrock surface, vertical offsets such as might be produced by faults, dipping strata boundaries, and various errors of interpretation and measurement. Examples of field data from two sites have been presented. Algorithms for the computation of seismic travel times and for contouring of the Meissner diagrams and anomaly diagrams by a digital computer have been presented in Appendix A.

Conclusions

56. On the basis of these studies, the following conclusions may be drawn:

a. Uphole refraction surveys and the presentation of data from them in Meissner diagrams are useful in exploration of the subsurface, but the correct interpretation of anomalous features is not straightforward. Interpretation can be aided by the use of anomaly diagrams, in which the travel time components contributed by the known or supposed nonanomalous conditions are subtracted out.

b. Variations in the depth of overburden have a disproportionately strong effect on travel times. The usefulness of the data and success in interpretation may depend upon the care given to detailing the configuration of the rock-overburden interface.

c. The sensitivity of the uphole refraction method to the presence of buried cavities is marginal, if travel times alone are used. Seismic travel times are affected by the presence of cavities and large cavities are detectable, but with the degree of resolution normally attained by contemporary instruments and field procedures, some cavities of a size great enough to be of engineering

significance (e.g., a tunnel 14 ft (4 m) across) are for practical purposes undetectable by means of travel time anomalies.

REFERENCES

Butler, D. K. and Murphy, W. L. 1980. "Evaluation of Geophysical Methods for Cavity Detection at the WES Cavity Test Facility," Technical Report GL-80-4, U. S. Army Engineer Waterways Experiment Station, Vicksburg, Miss.

Jackson, A. E., Jr., Ballard, R. F., Jr., and Phillips, B. R. 1979. "Geotechnical Investigations for MISERS BLUFF II: Results from the Subsurface Exploration Programs," Report to Defense Nuclear Agency by U. S. Army Engineer Waterways Experiment Station, Vicksburg, Miss.

Meissner, R. 1961. "Wave-Front Diagrams from Uphole Shooting," Geophysical Prospecting, Vol IX, pp 533-543.

Murrell, D. W. 1973. "Operation Dial Pack Project LN 305: Earth Motion and Stress Measurements in the Outrunning Region," Technical Report N-73-4, U. S. Army Engineer Waterways Experiment Station, Vicksburg, Miss.

Murrell, D. W. 1974. "Earth Motion and Stress Measurements, Project LN 302 Operation Dial Pack," Technical Report N-74-3, U. S. Army Engineer Waterways Experiment Station, Vicksburg, Miss.

Rockwell, D. W. 1967. "A General Wavefront Method," Seismic Refraction Prospecting, The Society of Exploration Geophysicists, P. O. Box 3098, Tulsa, Okla., pp 363-415.

Thornburgh, H. R. 1930. "Wave-Front Diagrams in Seismic Interpretation," Bulletin of the American Association of Petroleum Geologists, Vol 14, No. 2, pp 185-200.

U. S. Army Engineer Waterways Experiment Station. 1977. Symposium on Detection of Subsurface Cavities, Vicksburg, Miss.

APPENDIX A: COMPUTER-AIDED GENERATION OF WAVE-FRONT AND MEISSNER DIAGRAMS

Computation of Travel Times for the Wave-Front Diagram

1. In order to generate a wave-front diagram for a system of horizontal soil or rock layers or to obtain wave-front times to use in generating an anomaly diagram, it is necessary to compute the time required for a seismic signal to travel from a source location at the ground surface through a number of horizontal layers of various velocities to a fictitious buried detector (geophone) at some horizontal distance x and depth y. This appendix provides relations for the computation of that time in a form suitable for use with a digital computer.

2. The geometry of the travel time problem is shown in Figure A1. Suppose that there are ℓ horizontal layers with wave propaga velocities v_1, v_2, ... v_ℓ and thicknesses D_1, D_2, ... $D_{\ell-1}$, ∞. The shot point S is at the upper left corner, and the (fictitious) receiver R is in layer j at a depth y and horizontal distance x from S. In the example given in Figure A1, $\ell = 4$ and $j = 2$.

3. Two types of ray paths must be considered. The first, which will be called the "direct path," is illustrated by Path A in Figure A1. If R is in layer 1, the travel time for the direct path is given simply by

$$T = \frac{\sqrt{x^2 + y^2}}{v_1} \tag{A1}$$

If R is in a deeper layer, however, the geometry of the direct path is governed by Snell's law, which gives

$$\frac{\sin \alpha_i}{\sin \alpha_j} = \frac{v_i}{v_j} \tag{A2}$$

where α_1 is the direction of the path in any layer i lying above layer j and α_j is the direction of the path in layer j. The path is then fully described by the relation

$$x = \sum_{i=1}^{j-1} D_i \tan \alpha_i + \left(y - \sum_{i=1}^{j-1} D_i \right) \tan \alpha_j \qquad \text{(A3)}$$

or, substituting for α_i from Equation A2,

$$x = \sum_{i=1}^{j-1} D_i \tan \left[\sin^{-1} \left(\frac{v_i}{v_j} \sin \alpha_j \right) \right] + \left(y - \sum_{i=1}^{j-1} D_i \right) \tan \alpha_j \qquad \text{(A4)}$$

Since a chosen combination of x and y is under consideration, the unknown in this equation is α_j. This must be determined by trial, since an explicit method of solving for it is not known, at least to the author. Once α_j has been found and the α_i's computed from Equation A2, the travel time T can be computed from the equation

$$T = \sum_{i=1}^{j-1} \frac{D_i}{v_i \cos \alpha_i} + \frac{\left(y - \sum_{i=1}^{j-1} D_i \right)}{v_j \cos \alpha_j} \qquad \text{(A5)}$$

which, like Equation A3, can be verified by inspection of Figure A1.

4. The second type of path that must be considered is one that is critically refracted at an interface deeper than R. One such path is shown in Figure A1 as Path B. Suppose that the deepest part of the refracted path is in some layer k; the direction angle β_k of the path in layer k is therefore 90 deg, and application of Snell's law gives the direction angle β_i in any overlying layer i as

$$\sin \beta_i = \frac{v_i}{v_k} \qquad \text{(A6)}$$

The length u of the horizontal segment of the path that lies in layer k is given by

$$u = x - \left\{ \sum_{i=1}^{k-1} D_i \tan\left(\sin^{-1}\frac{v_i}{v_k}\right) + \sum_{i=j+1}^{k-1} D_i \tan\left(\sin^{-1}\frac{v_i}{v_k}\right) + \left[\left(\sum_{i=1}^{j} D_i\right) - y\right] \tan\left(\sin^{-1}\frac{v_j}{v_k}\right)\right\} \tag{A7}$$

The length of a segment in the path in layer i is equal to $D_i/\cos\beta_i$; so the total travel time T is

$$T = \frac{u}{v_k} + \sum_{i=1}^{k-1} \frac{D_i}{v_i \cos\left(\sin^{-1}\frac{v_i}{v_k}\right)} + \sum_{i=j+1}^{k-1} \frac{D_i}{v_i \cos\left(\sin^{-1}\frac{v_i}{v_k}\right)} + \frac{\left[\left(\sum_{i=1}^{j} D_i\right) - y\right]}{v_j \cos\left(\sin^{-1}\frac{v_j}{v_k}\right)} \tag{A8}$$

Two further conditions are required for Equations A7 and A8 to be applicable: (a) the velocity v_k of layer k must be greater than the velocities v_i of all shallower layers in order for Equation A7 to give a real value for u; and (b) u must be positive to be physically meaningful. Thus, it is necessary to compute the refracted path travel time for each layer k for which

a. $k > j$
b. $v_k > v_i$ for all i less than k
c. $u > 0$

Of the set of the various travel times computed in this way (by Equation A8), in addition to the travel time computed according to Equation A5 (or Equation A1, if it applies), the smallest is the time of the first arrival, which is the time value applicable to point R.

5. In the case of an uphole refraction survey, the points R form an m by n array, where m is the number of geophone stations and n is the number of shot points. The set of shot point depths thus forms a one-dimensional array y_1 , y_2 , ... y_n , and the set of geophone distances a one-dimensional array x_1 , x_2 , ... x_m . For a hypothetical Meissner diagram, these values may be generated at equal intervals or values corresponding to those that actually occurred under field conditions may be used. The value of x_1 may be taken as zero, if desired, to represent a geophone at the top of the borehole, and the value of y_1 as zero to represent a shot point at the top of the borehole. Since both the shot and the geophone are imaginary, no damage to equipment will be incurred.

6. A flowchart for the computation of seismic travel times for a horizontally layered earth is given in Figure A2. The algorithm described by this flowchart includes solution of Equation A3 by iteration and the determination of the minimum travel time. An m by n array of travel times, designated T (M, n) , is generated, and provision must be made for dimensioning of this array as well as other arrays that are listed in the beginning READ block of the flowchart. Output of the values generated is not shown in the flowchart, but if a printed output is desired, output coding can be inserted immediately before the END statement. Details of input, output, and "housekeeping" functions will depend on the computer and programming language used.

Computer-Generated Contours

7. A very simple and unsophisticated method can be used to produce contour maps from gridded data on any computing system with graphics capability. The contouring routine uses a straightforward linear interpolation between data points to draw contours of equal values of a quantity z that varies in some manner over the x-y plane. In contouring a Meissner diagram from field data, values of z represent seismic travel times observed in the field; for a wave-front diagram representing a hypothetical layered system, values of z are equated

to the time values T computed as described in the preceding paragraphs. A value of z might also represent the elevation of a point whose geographical location is given by the rectangular coordinates x, y . The contour plot would then be a topographic map of the surface $z = f(x, y)$.

8. The algorithm requires that a value of z be specified at each point (node) of a regular grid on the x-y plane. In principle, the grid does not have to be strictly rectangular, so long as the number of nodes in each row and column is uniform and they form an orderly sequence of quadrilateral elements (see Figure A3). In a Meissner diagram, however, a rectangular grid is generated by the locations of the shot points on one side of the area to be contoured and the geophone stations on a second side. This simplifies the input data somewhat, since the grid is defined by the two one-dimensional arrays of shot point elevations and geophone locations.

9. The routine deals separately and independently with successive quadrilaterals of which the grid points are the corners. The contouring within each quadrilateral element is done on the basis of interpolation between the values at the four corner nodes. In Figure A4, points 1, 2, 3, and 4 represent the locations of four nodes on the topographic surface, and 1', 2', 3', and 4' represent their positions projected on the x-y plane. First, an additional point is generated at the centroid (point 0') of the quadrilateral, and the arithmetic mean of the four nodal values of z is taken to be the value of z at point 0, which is assumed to lie on the topographic surface. The coordinates of point 0 are given by

$$\begin{aligned} x_0 &= 1/4\ (x_1 + x_2 + x_3 + x_4) \\ y_0 &= 1/4\ (y_1 + y_2 + y_3 + y_4) \\ z_0 &= 1/4\ (z_1 + z_2 + z_3 + z_4) \end{aligned} \tag{A9}$$

The surface can now be approximated by the four triangular plates 1-2-0, 2-3-0, 3-4-0, and 4-1-0. Since each triangular plate is plane, any contour on it is a line segment. The contour is produced by finding

the two points where the plate's edges pass through the contour value and then drawing a straight line between them. Each of the four triangular plates is contoured in succession, and the process then moves to the quadrilateral defined by the next set of grid points.

10. The algorithm for this operation is further described in the flowchart in Figure A5. As mentioned earlier, the array z may be equated to T, to plot a wave-front diagram from computed travel times, or it may be input to the program as observed data. The graphic function is represented in the flowchart in very general form as a DRAW operation, in which a line segment is drawn from the point x_p, y_p to the point x_q, y_q. The form of the coding for this operation will depend on the computer and the programming language used. Provision for scaling the plot, not shown in the flowchart, must also be provided in a form appropriate to the computer and the programming language. Supplementary graphical operations, such as plotting the node points, labeling, and the like, are also omitted from the flowchart.

11. The contour map produced by this routine has a somewhat mechanical appearance, which can, however, be improved by finer division of the grid. Maps generated so far have been relatively free of spurious features, though knife-edge contours or branching of contours may appear where adjacent grid points lie at the same contour value. Such features are mathematically possible, but are normally excluded from contour maps by convention. If these effects are considered objectionable, they can be eliminated by hand-tracing and smoothing the computer-generated contours.

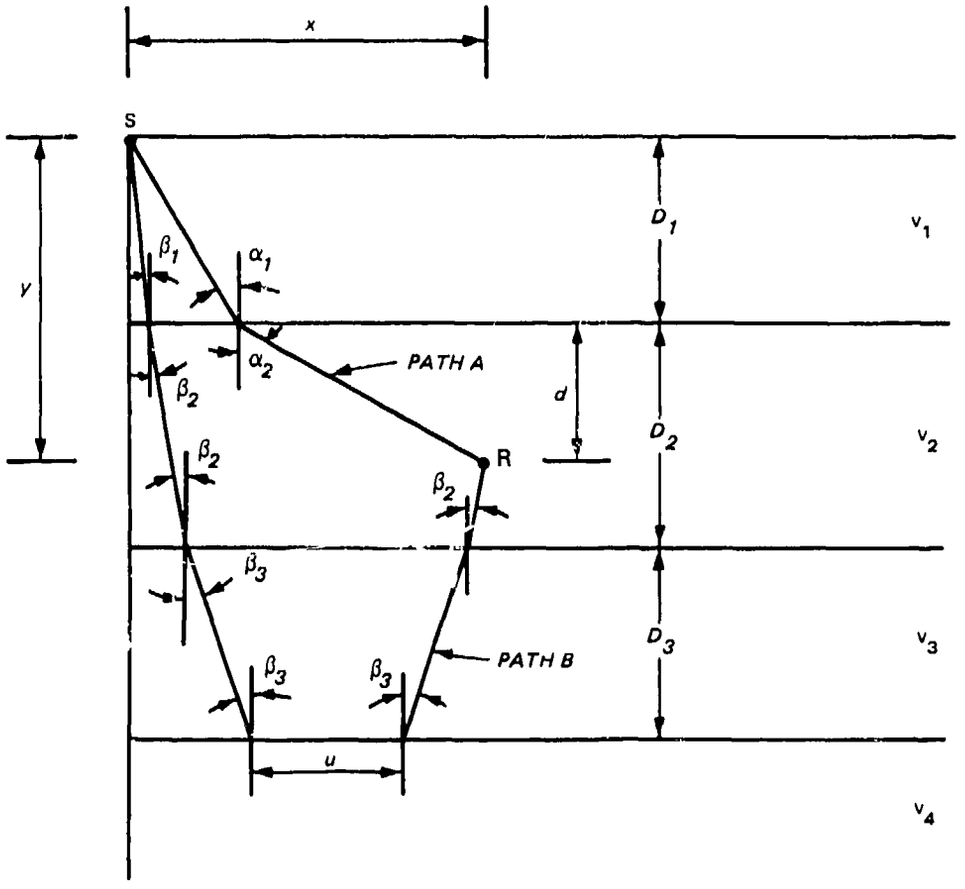

Figure A1. Geometry of the travel time problem

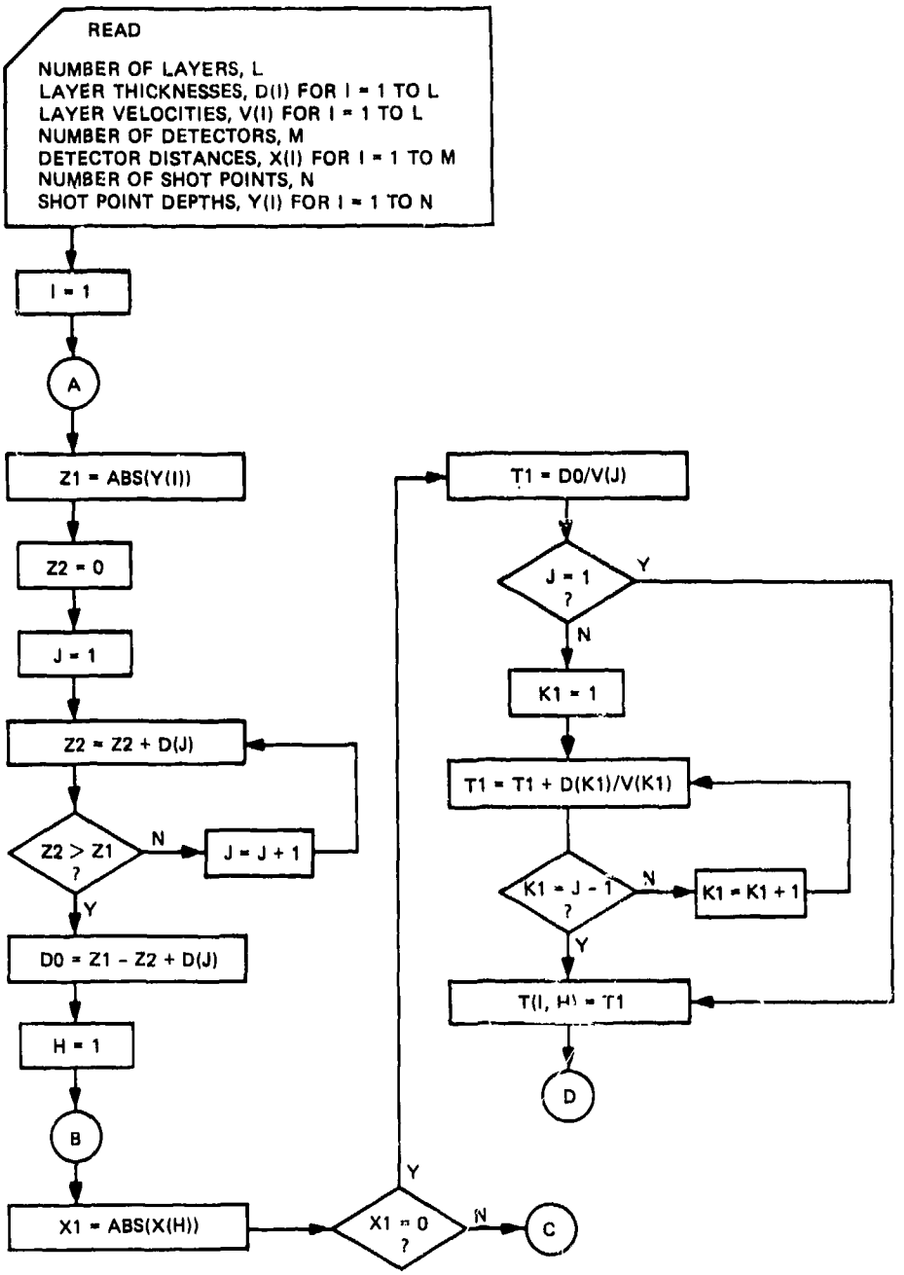

Figure A2. Flowchart for computation of travel times of seismic signal between shot points in a borehole and detectors on ground surface, for a horizontally stratified earth (Sheet 1 of 6)

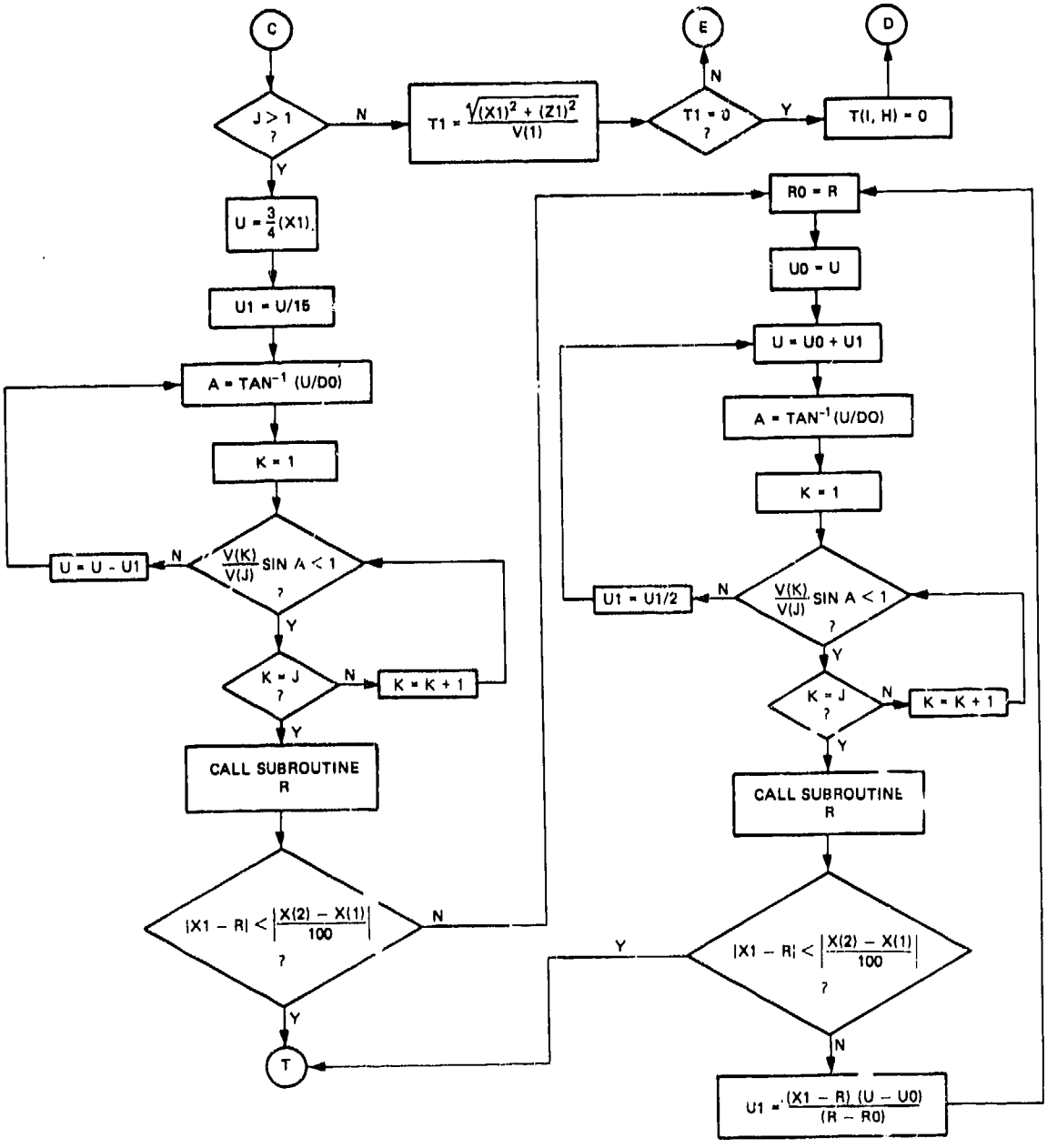

Figure A2. (Sheet 2 of 6)

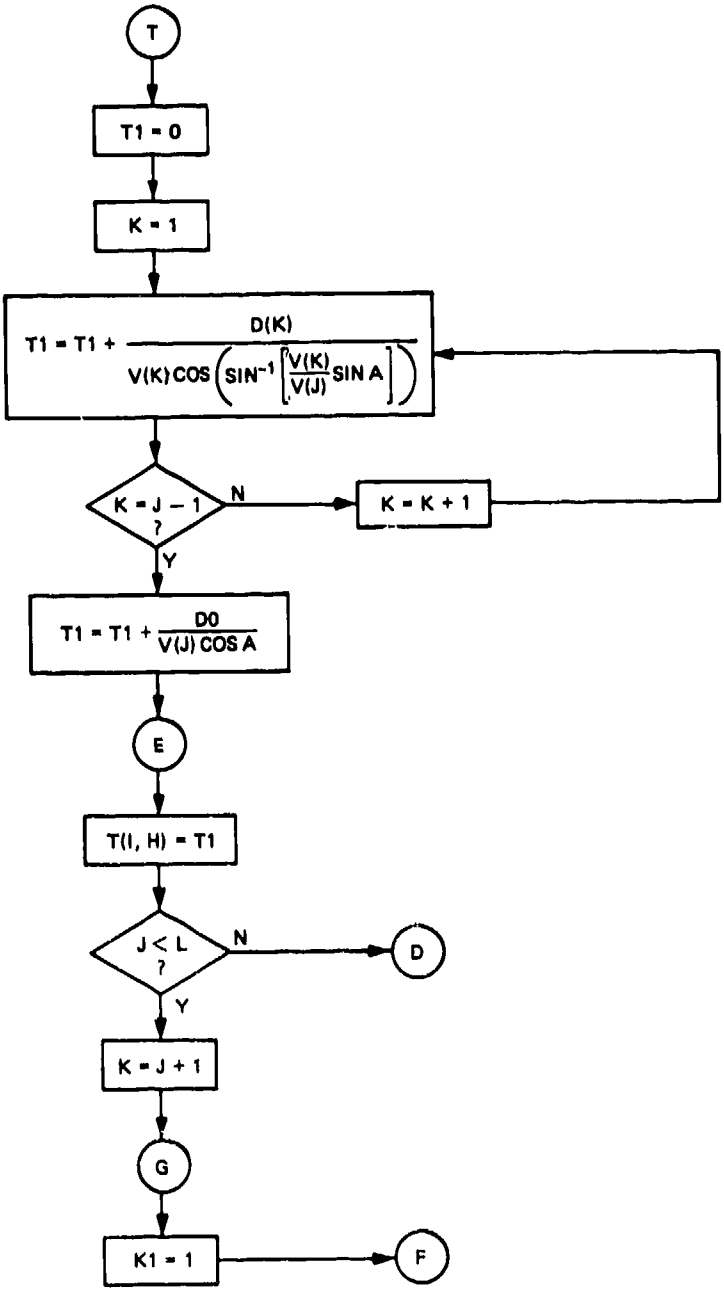

Figure A2. (Sheet 3 of 6)

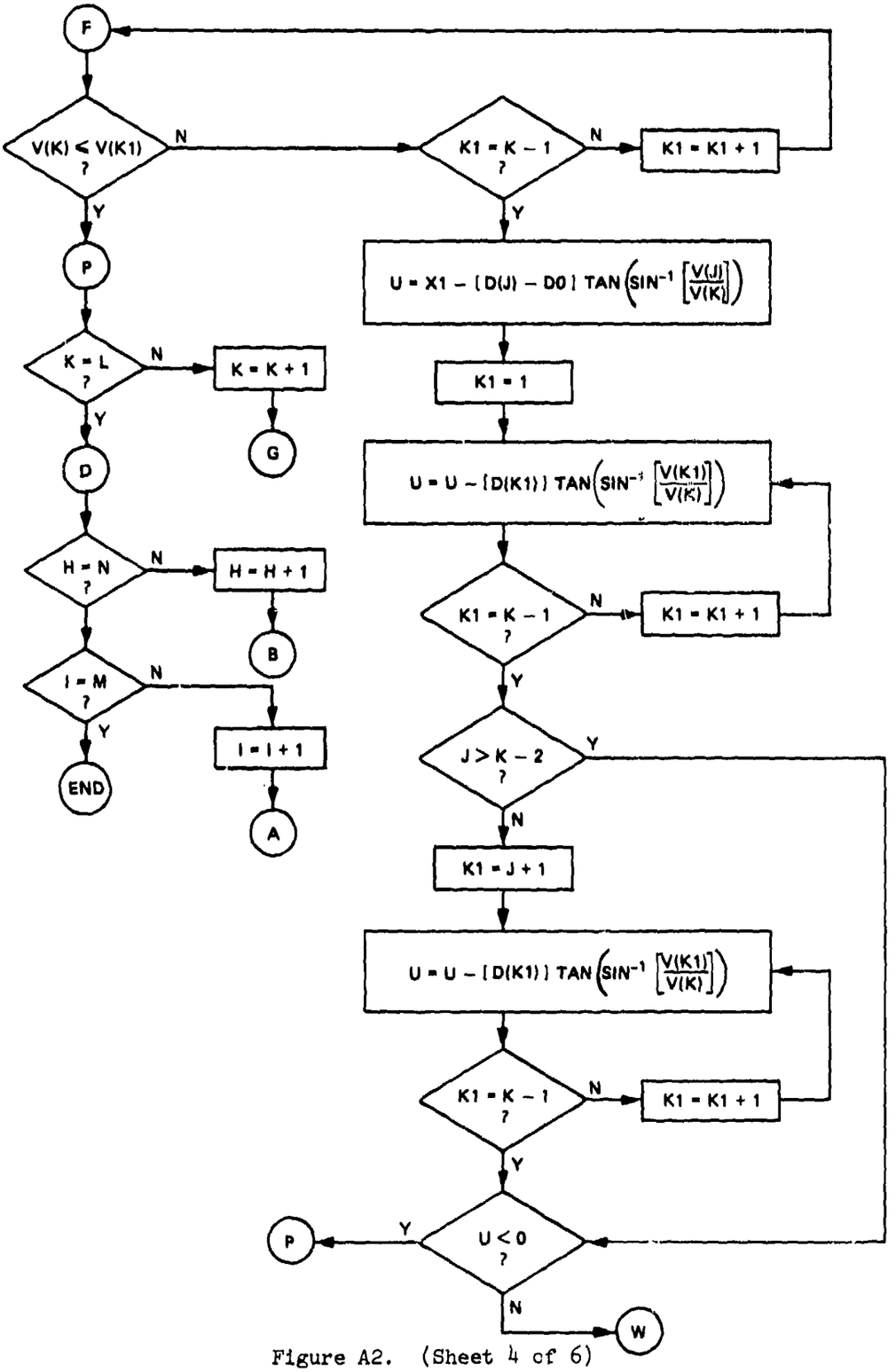

Figure A2. (Sheet 4 of 6)

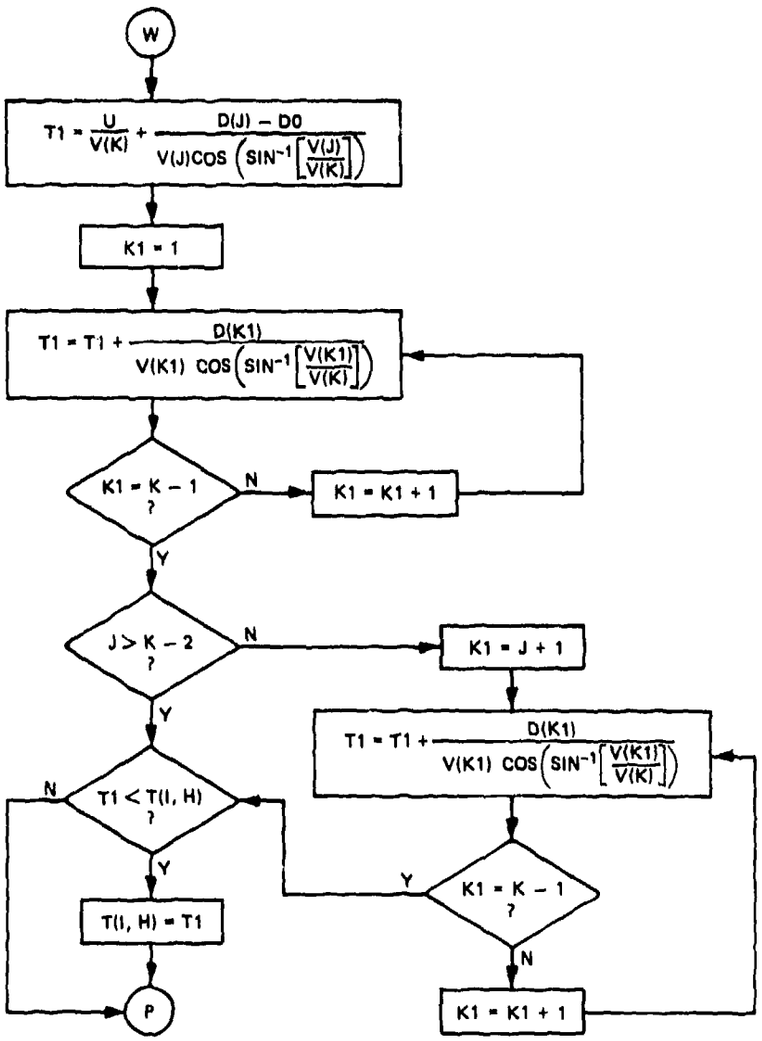

Figure A2. (Sheet 5 of 6)

SUBROUTINE R

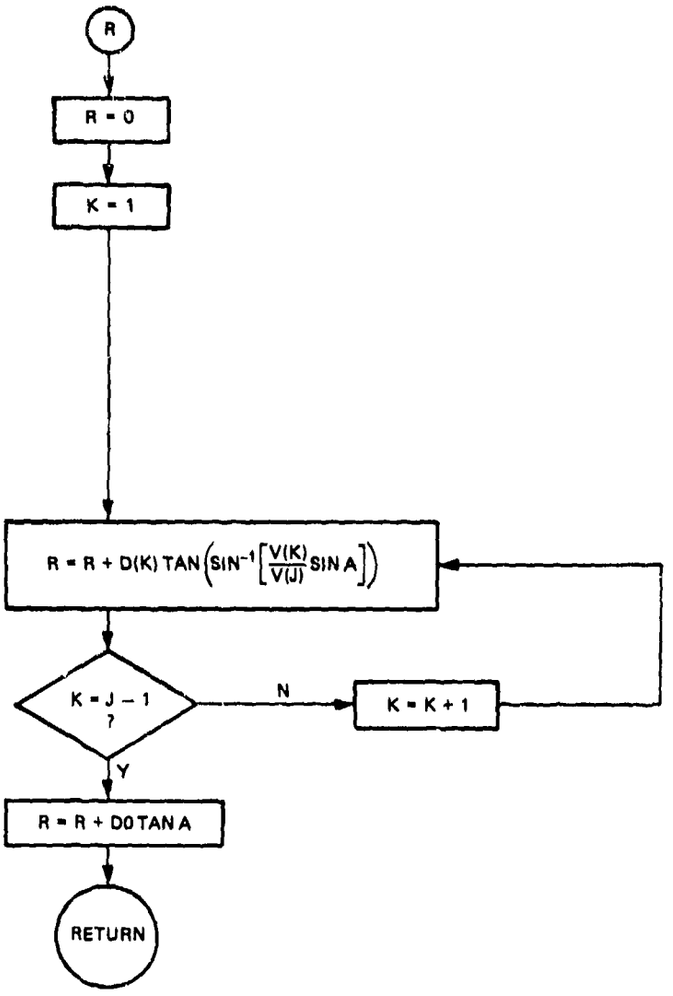

Figure A2. (Sheet 6 of 6)

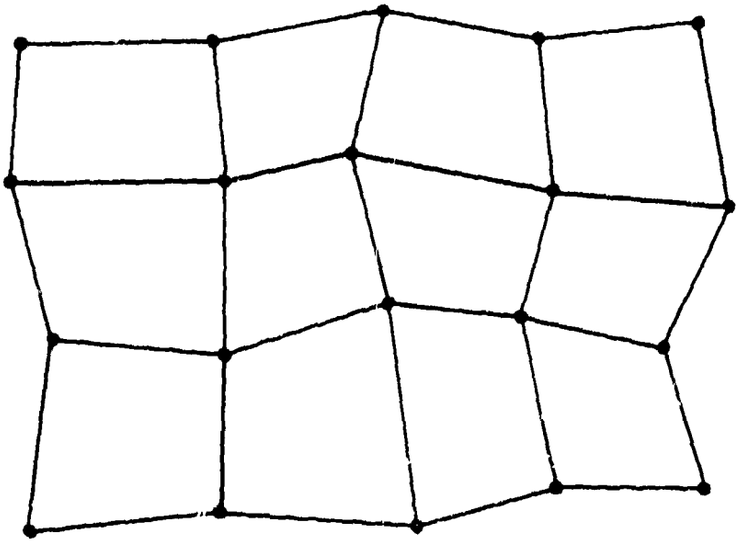

Figure A3. Quadrilateral grid for contouring of gridded data

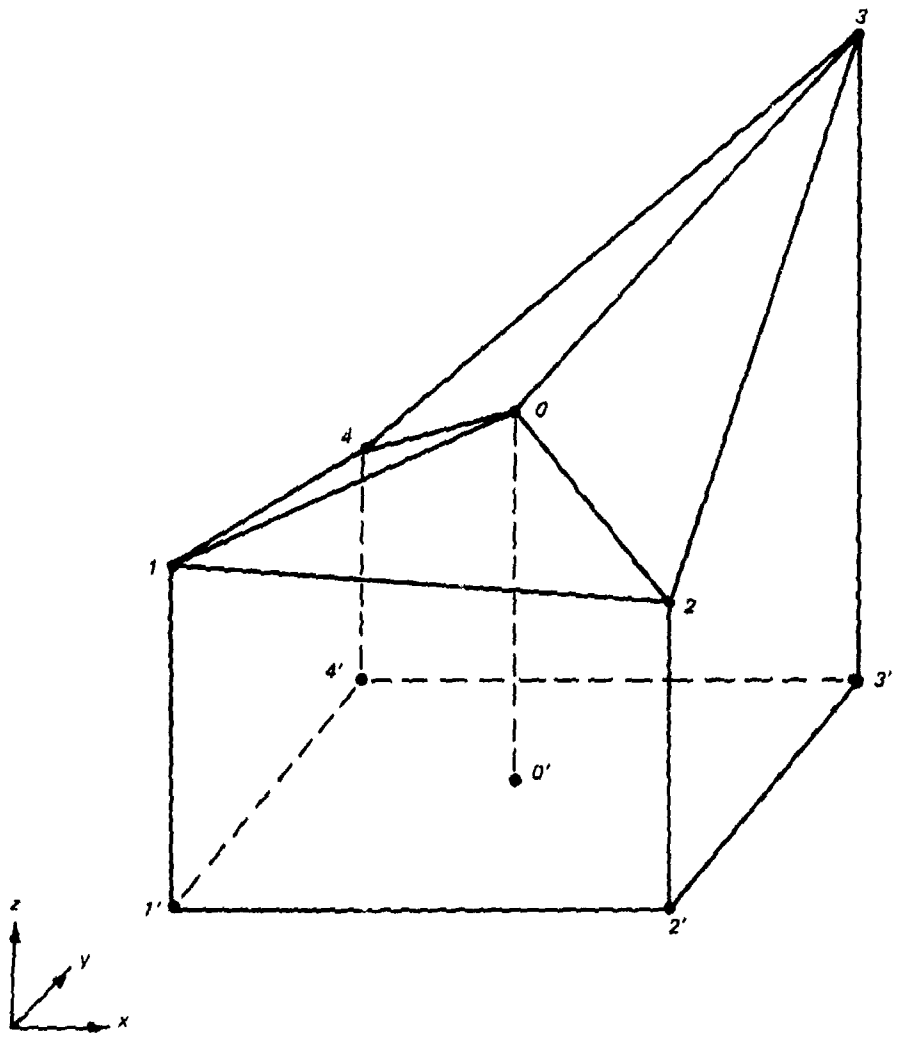

Figure A4. Representation of topographic surface by triangular plates

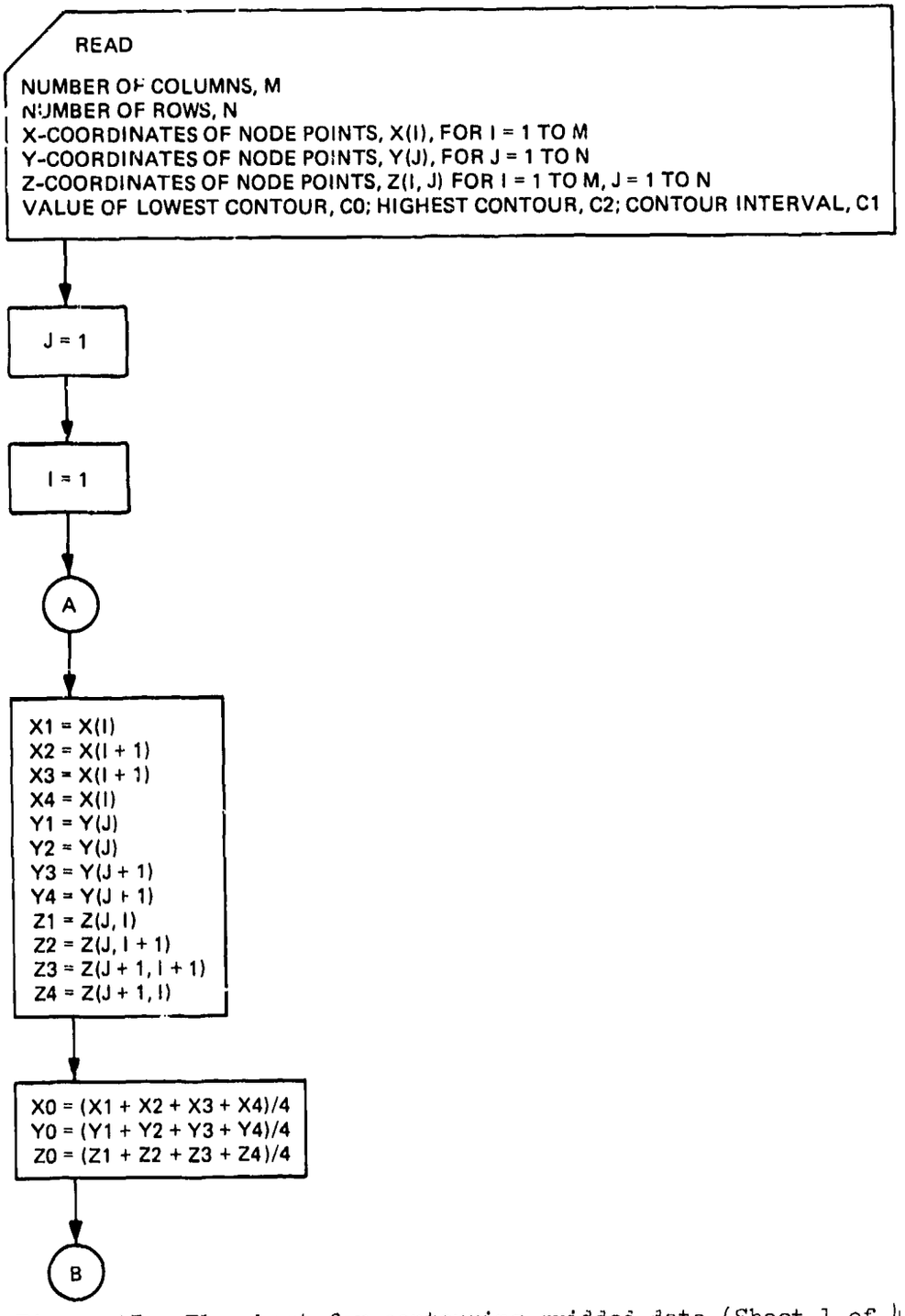

Figure A5. Flowchart for contouring gridded data (Sheet 1 of 4)

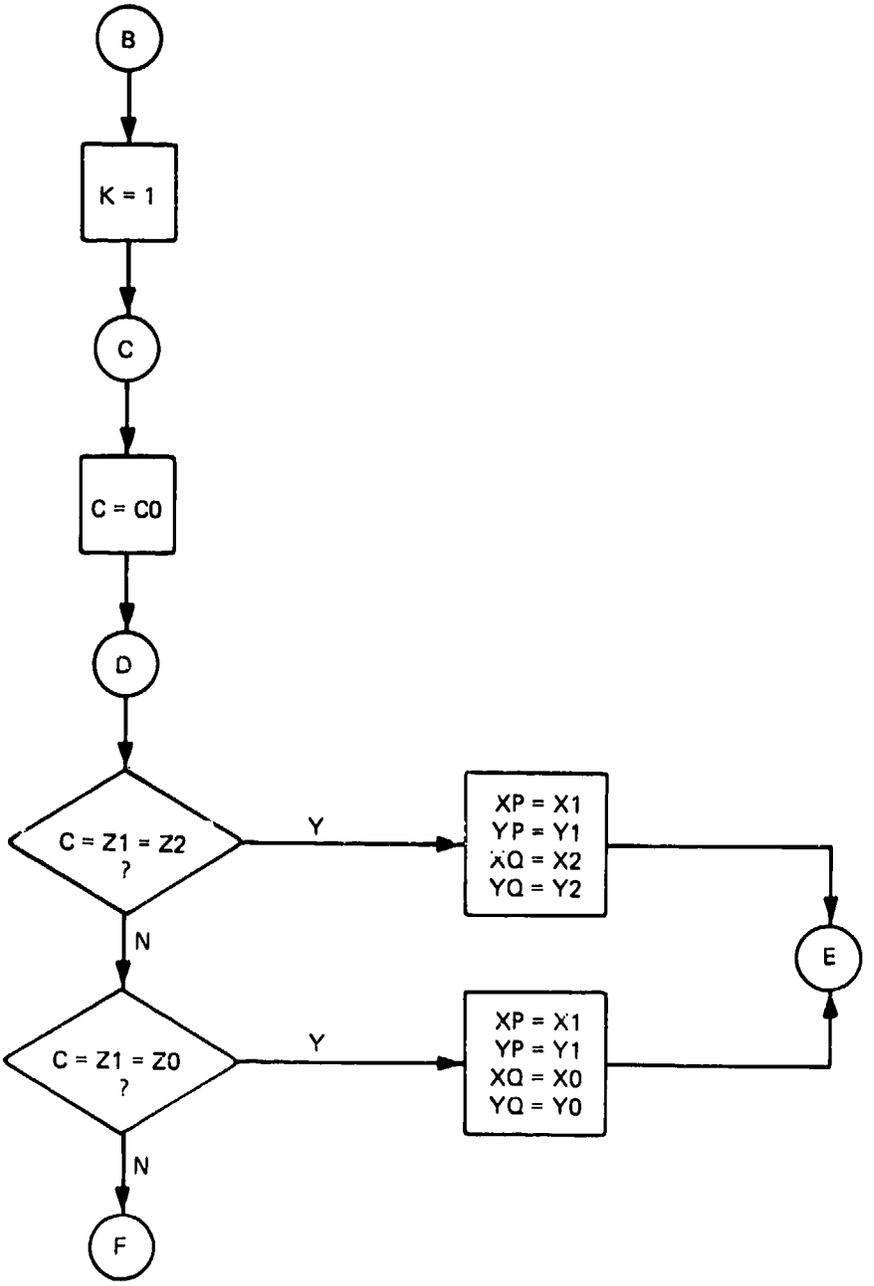

Figure A5. (Sheet 2 of 4)

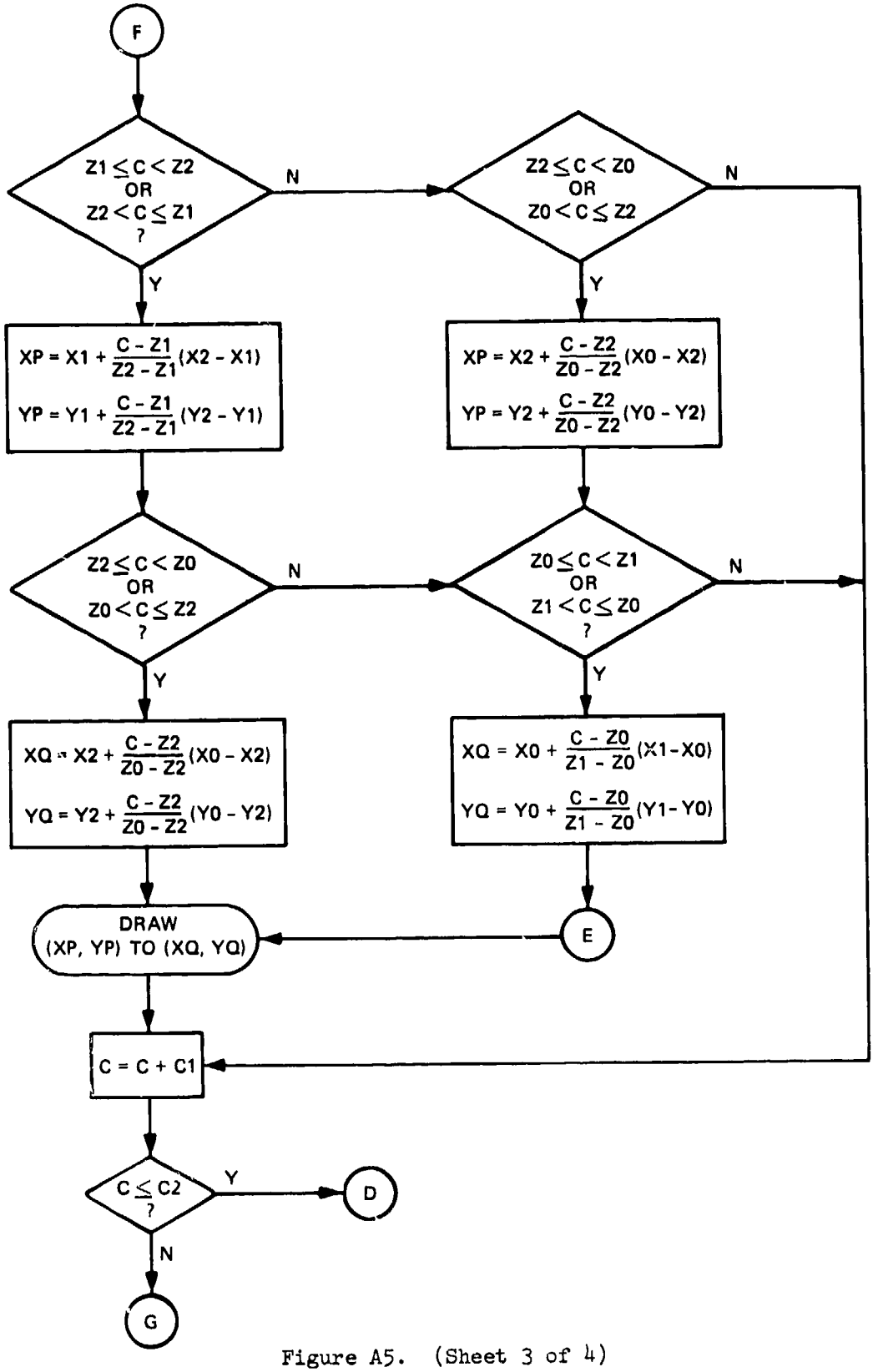

Figure A5. (Sheet 3 of 4)

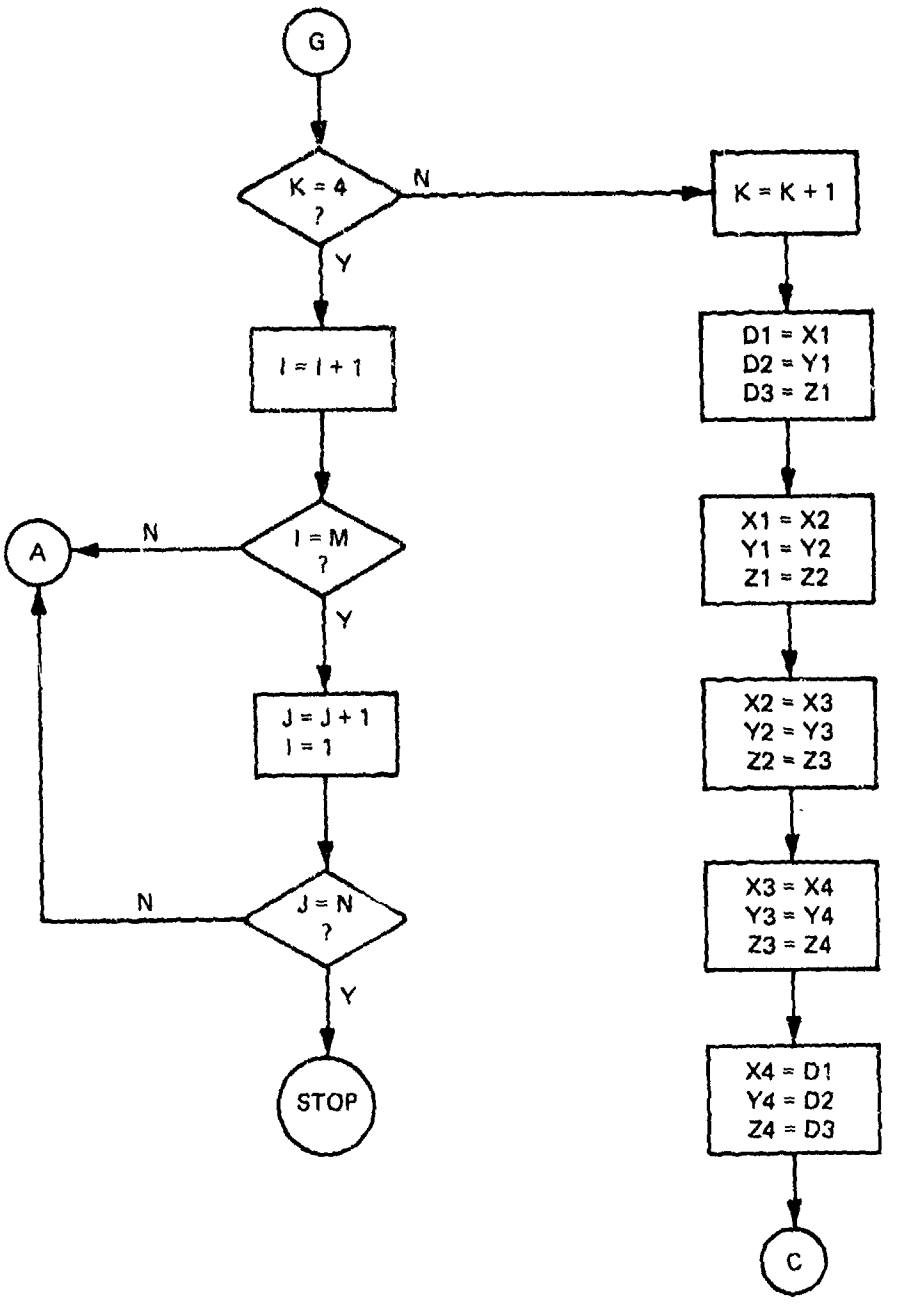

Figure A5. (Sheet 4 of 4)

In accordance with letter from DAEN-RDC, DAEN-ASI dated 22 July 1977, Subject: Facsimile Catalog Cards for Laboratory Technical Publications, a facsimile catalog card in Library of Congress MARC format is reproduced below.

Franklin, Arley Graves
Interpretation of data from uphole refraction surveys / by Arley G. Franklin. Vicksburg, Miss. : U. S. Waterways Experiment Station ; Springfield, Va. : available from National Technical Information Service, 1980.
49, 19 p. : ill. ; 27 cm. (Miscellaneous paper - U. S. Army Engineer Waterways Experiment Station ; GL-80-5)
Prepared for Office, Chief of Engineers, U. S. Army, Washington, D. C., under CWIS Work Unit 31150.
References: p. 49.

1. Refraction. 2. Seismic refraction. 3. Seismic refraction method. 4. Seismic surveys. 5. Subsurface exploration. 6. Uphole refraction. I. United States. Army. Corps of Engineers. II. Series: United States. Waterways Experiment Station, Vicksburg, Miss. Miscellaneous paper ; GL-80-5.
TA7.W34m no.GL-80-5